ABSTRACT

DAN, CHEN. Ligand Dynamics, Recognition and Structure/Function Relationships of Bio-nanoparticles. (Under the direction of Dr. Alex I. Smirnov).

Surface functionalized gold nanoparticles have been actively researched for many applications in life sciences and biomedicine over the last decade. Polyfunctional water soluble Au nanoparticles (Au NPs) demonstrated their potential in the imaging of biomolecular processes, biosensing, drug delivery and development of new bio-inspired materials. [1 2] It is now well documented that biorecognition properties of Au NPs could be tuned by choosing proper monolayer terminal groups, opening new opportunities in biological and biomedical applications. [3]

However, detailed understanding of structure and dynamics of the nanoparticles' ligand layer – an essential pre-requisite for further development of Au NPs applications - is still missing in the literature. Specifically, there is no full understanding of the dynamics of self-assembled monolayers and the ns scale fluctuations of individual molecules; the local electrostatics and hydrogen bonding at the bionanoparticle interface are also scarcely reported. The main research aims of this project were to combine the advantages of the synthesis of novel spin labels and probes and methods of spin labeling EPR with development of EPR spectroscopic methods for assessing dynamics, structure, and electrostatic properties of bio-nanoparticle interfaces.

In this project, we synthesized small water-soluble Au NPs protected by ligands bearing protonatable terminal groups (amino groups) so the nanoparticle net charge could be changed

as the pH of the medium changed. Disulfide and thioacetate ligands modified with both ionizable and non-ionizable nitroxides were synthesized and employed for spin-labeling of Au NPs through ligand exchange reactions. Basic functionalities of ionizable nitroxide participate in proton-exchange reactions and report on the pH of the environment through changes in the EPR spectral parameters, *e.g.*, nitrogen hyperfine coupling constants and electronic g factors, as well as through the variations in order parameters. pK_a's of the ligands modified with pH-sensitive nitroxide were experimentally determined both in solution and at the nanoparticle interface and these ligands were proposed to be useful for EPR studies of the electrostatics and proton transfer-related phenomena at charged nanoparticle/biomolecule interface.

Ligand Dynamics, Recognition and Structure/Function Relationships of Bio-nanoparticles

by
Dan Chen

A thesis submitted to the Graduate Faculty of
North Carolina State University
in partial fulfillment of the
requirements for the degree of
Master of Science

Chemistry

Raleigh, North Carolina

2014

APPROVED BY:

_____	_____
Dr. Alex I. Smirnov Committee Chair	Dr. Yaroslava G. Yingling
_____	
Dr. Gufeng Wang	

BIOGRAPHY

Dan Chen was born on Sept. 30th, 1987 in Mianyang, China, where she spent her first 18 years of the life and found herself interested in science. Then she followed her heart to learn more about physics and chemistry in the University of Science and Technology of China and got her B.S. degree there. After that, Dan continued her research in Physical Chemistry under the direction of Dr. Alex I. Smirnov at North Carolina State University.

ACKNOWLEDGMENTS

There are so many people I would love to acknowledge. I would like to express my deepest appreciation to my thesis advisor Prof. Alex I. Smirnov, you have backed me up through my graduate life and my future career. Without your encouragement and support on my research this thesis would not have been possible. I would also like to thank Prof. Gufeng Wang and Prof. Yaroslava G. Yingling for serving as my committee members.

My sincere thanks also go to Dr. Maxim A. Voinov in our group for all the advices and help on my research. Thank you for your patience and guidance on all the synthesis skills.

Thank everyone in Smirnov and Smirnov groups for all the days we worked together and all the fun we had.

TABLE OF CONTENTS

LIST OF TABLES

LIST OF FIGURES

LIST OF ABBREVIATIONS

AIBN	Azobisisobutyronitrile
DCC	N,N'-Dicyclohexylcarbodiimide
DMAP	4-Dimethylaminopyridine
DLS	Dynamic light scattering
DMSO	Dimethyl sulfoxide
DMF	Dimethylformamide
EPR	Electron paramagnetic resonance
IR	Infrared spectroscopy
NMR	Nuclear magnetic resonance
THF	Tetrahydrofuran
TLC	Thin layer chromatography
TEM	Transmission electron microscopy

CHAPTER 1 INTRODUCTION

1.1 Electron Spin Resonance

In 1922, two German physicists, Otto Stern and Walther Gerlach, carried out one of the most important and fundamental experiment in quantum mechanics. In Stern-Gerlach experiment, atoms could only have certain discrete orientations when passing through an inhomogeneous magnetic field, which indicated the existence of electron spin. This experiment led to development of the concept of spin in quantum mechanics, and, ultimately, several decades later, to discovery of magnetic resonance – both nuclear magnetic resonance (NMR) and electron paramagnetic resonance (EPR).

When a magnetic moment μ is exposed to a magnetic field B, it has energy

$$E = -\mu \bullet B = -\mu B \cos(\mu, B) \tag{1.1}$$

In quantum mechanics, this equation can also be expressed as

$$\hat{H} = -\hat{\mu} B \tag{1.2}$$

According to Dirac's formulation of quantum mechanics, $\hat{H}$ is the Hamiltonian operator, corresponding to the total energy of the system. $\hat{\mu}$, the magnetic momentum operator, is proportional to the spin angular momentum $\hat{s}$,

$$\hat{\mu} = g\gamma_e \hat{s} \tag{1.3}$$

γ_e is called the magnetogyric ratio,

$$\gamma_e = -\frac{e}{2m_e} \tag{1.4}$$

And g is called the $g - factor$ of electron, which is very close to 2. The exact value of *g-factor* reflects some intrinsic properties (structure) of the radicals. For free electrons, $g_e = 2.0023$.

In magnetic resonance magnetic field B is always taken along z-direction. The component of spin angular momentum along this direction is

$$\hat{\mu}_z = g\gamma_e \hat{s}_z \tag{1.5}$$

thus

$$\hat{H} = -\hat{\mu}_z B = -g\gamma_e \hat{s}_z B \tag{1.6}$$

For spin s=1/2, the eigenvalue of $\hat{s}_z$ is $m_s\hbar$ with $m_s = \pm\frac{1}{2}$, and, accordingly, the total energy of an electron in magnetic field B is

$$E_{m_s} = -g\gamma_e m_s \hbar B = g\mu_B m_s B \tag{1.7}$$

The Bohr magneton, μ_B, is defined as

$$\mu_B = -\gamma_e \hbar = \frac{e\hbar}{2m_e} = 9.724\times10^{-24}\, JT^{-1} \tag{1.8}$$

As a result, states of different m_s values would be degenerate in the absence of magnetic field and the degeneracy will be removed by applying magnetic field B. Two energy levels are formed with the gap given as (see also Figure 1) :

$$\Delta E = E_\alpha - E_\beta = g\mu_B B \tag{1.9}$$

The existence of these energy levels can be probed by applying a radiofrequency field with frequency ν to cause $\alpha \rightarrow \beta$ transition at the resonance conditions:

$$h\nu = g\mu_B B \tag{1.10}$$

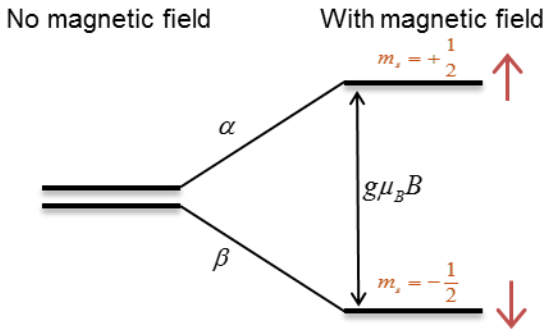

Fig. 1.1 Energy levels of s=1/2 spin in presence and absence of magnetic field and the resonance conditions (redrawn from reference 4)

Electron spin resonance is a spectroscopic technique studying molecular species with unpaired electrons by analyzing the magnetic fields that in resonance with monochromatic (microwave or millimeter wave) radiation. The magnetic field applied in a typical commercial EPR spectrometer is around 0.3 T, thus, the resonating frequency of electromagnetic field is around 10 GHz, corresponding to wavelength within microwave range (wavelength of about 2 cm).

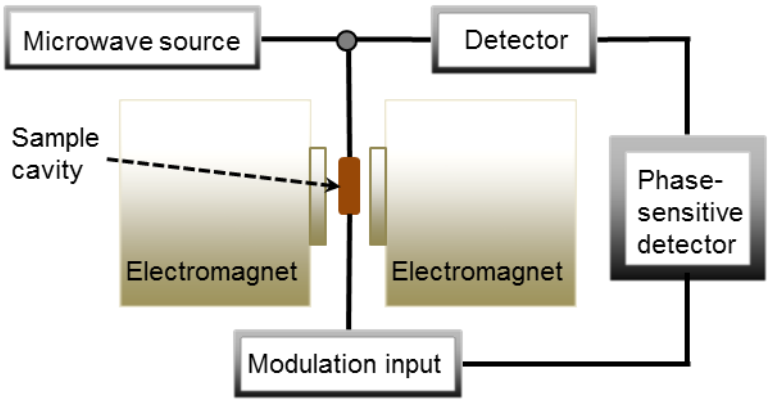

Fig. 1.2 The layout of a continuous-wave EPR spectrometer (redrawn from reference 4)

In continuous wave (CW) EPR experiment the EPR spectrm is detected using phase-sensitive detection when magnetic field is modulated at *ca.* 100 kHz. Then the detected EPR spectrum is the first-derivative of absorption. A typical spectrum of free nitroxide radicals is shown below in Fig. 1.3.

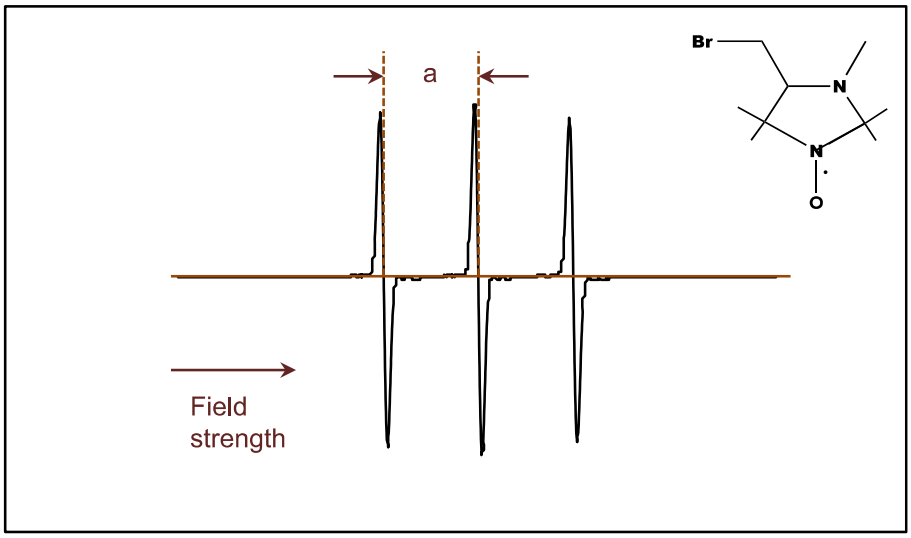

Fig. 1.3 A typical EPR spectrum for free nitroxide radicals.
a is the nitrogen hyperfine splitting of the spectrum. The position of the central line is determined by equation $B = \frac{h\nu}{g\mu_B}$.

The hyperfine splitting is a very important property of EPR. It arises from two aspects. Firstly, for *p*-orbital electrons, the hyperfine splitting is caused by magnetic dipole-dipole interaction between electron spin and the nuclear spin present in vicinity. This dipolar interaction is anisotropic and can be averaged out by molecular motion. Secondly, for *s*-orbital electrons, there is an isotropic Fermi contact interaction. Due to these interactions, local fields are formed and vectorially added to the external field. As the consequence, the effective field is

$$H_{eff} = H + H_{local} = H + am_I \tag{1.11}$$

a is the hyperfine splitting constant, which has different values for different nuclei, and m_I is the nucleus spin quantum number. Details of some nuclides are listed in the table 1.1.

Table 1.1 Spin Numbers and Hyperfine Splitting Constants [4]

Nuclide	Spin I	m_I	Hyperfine splitting constant	
			Isotropic coupling	Anisotropic coupling
^{1}H	$\frac{1}{2}$	$\pm\frac{1}{2}$	50.8(1s)	
^{2}H	1	$0, \pm 1$	7.8(1s)	
^{14}N	1	$0, \pm 1$	55.2(2s)	3.4(2p)

As a result, the energy levels will be further split by this electron-nucleus interaction, as shown in Fig. 1.4.

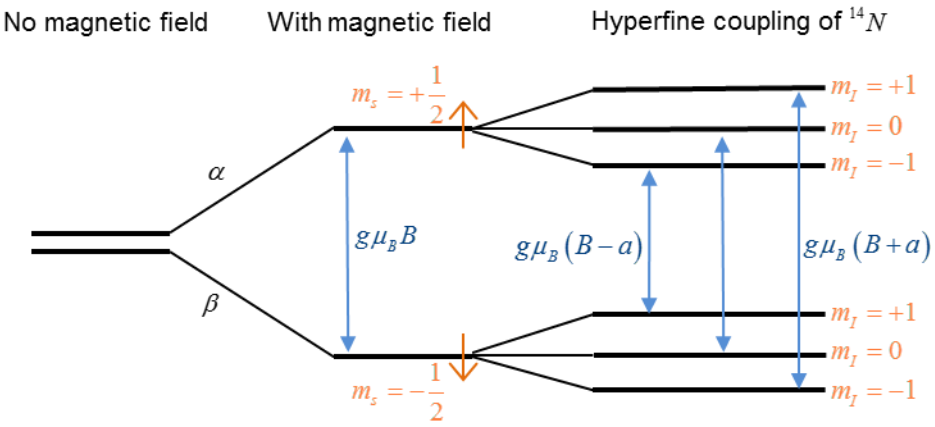

Fig. 1.4 Hyperfine interaction between an electron and a ^{14}N nucleus.

The resulting EPR spectrum is shown in Fig. 1.3. The intensities of every peak are the same (redrawn from reference 4).

1.2 Nitroxide Radicals

Nitroxide radicals is a family of organic persistent free radicals containing an unpaired electron delocalized between nitrogen and oxygen atoms of the nitroxide group (N–O•). Spin quantum number of the most abundant ^{16}O oxygen isotope of the N–O•

group is 0, so it has only one allowed nuclear spin state which results in no hyperfine interactions with the unpaired electron. However, the spin quantum number of nearby nitrogen nucleus (^{14}N) could be 0 or ±1 (table 1.1). Because of the magnetic dipole-dipole interaction between electronic spin and the nitrogen nuclear spin, hyperfine structure of the three absorption lines is observed in the EPR spectra of nitroxide radicals (Fig. 1.3). Chemical structures of representative nitroxides are shown in Fig. 1.5.

Nitroxide radicals attached to other molecules or biopolymer chains act as spin probes. When tumbling freely, spin probes give an EPR spectrum similar to that shown in Fig. 1.3. However, once the local enviroment changes, their movements could be restricted, and the lineshapes would be dramatically affected, providing information on dynamic properties of spin probes and their immediate molecular enviroment.

In this project, the following nitroxide radicals (Fig. 1.5) were employed. 3-Carboxy-2,2,5,5-tetramethyl-3-pyrroline-1-oxyl (**1**, Fig. 1.5) is used to study the dynamics of the self-assembled monolayers. **1** is not intrinsically sensitive to the pH of the medium since it does not contain an ionizable group in the vicinity of the N–O• group (*note: COOH group is too far from the N–O• group to noticeably affect its magnetic parameters*).

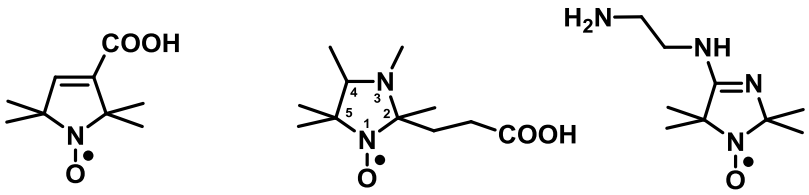

Fig. 1.5. Chemical structures of the nitroxides used in this project.

2-(2-Carboxyethyl)-2,3,4,5,5-pentamethylimidazolidine-1-oxyl (**2**, Fig. 1.5) and 4-(2-Aminoethylamino)-1-oxyl-2,2,5,5-tetramethyl-2,5-dihydro-1H-imidazole (**3**, Fig. 1.5) are pH-sensitive nitroxide radicals. Nitroxide **2** has a tertiary amino group at position 3 of the imidazolidine heterocycle, which could protonated or nonprotonated in different environment. Nitroxide **3** has a protonatable amidino group as a part of the heterocycle that can report on its ionization state of the molecule through the changes in magnetic parameters (*e.g.*, isotropic nitrogen hyperfine coupling constant, A_{iso}, or electronic *g*-factor), or order parameters. Functional groups in the side chains of the nitroxides **1-3** can be used as attachment sites for molecules of interest.

When attached to the ligands, nitroxides **2** and **3** act as spin probes and parameters of their EPR spectra (*e.g.,* A_{iso}) report on the ionization state of corresponding spin-labeled ligands. Monitoring how A_{iso} changes with pH allows one to determine the pK_a of the ionizable group of the nitroxide in the spin-labeled ligand. Fig. 1.6 shows an example how the X-band (9.5 GHz) EPR spectra of the ligand modified with the nitroxide **2** change with pH in buffer solutions containing 40 v/v% of isopropanol.

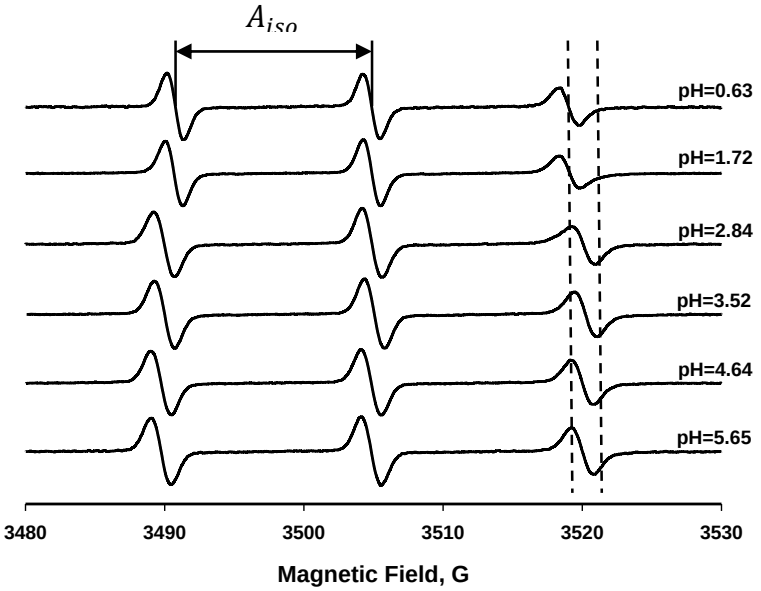

Fig. 1.6 Representative room-temperature X-band EPR spectra of 2-(2-Carboxyethyl)-2,3,4,5,5-pentamethylimidazolidine-1-oxyl-modified ligand in a series of buffer solutions containing

40% of isopropanol. pH values of the solutions are indicated next to the corresponding spectra. Dashed lines mark approximate positions of the high-field nitrogen hyperfine coupling components corresponding to protonated and nonprotonated forms of the nitroxide.

1.3 Gold Nanoparticles (Au NPs)

Gold is one of the most widely studied metals in the world. Besides its aesthetic and collectible values, it also plays an important role in scientific research.

During the past decade polyfunctional water soluble Au NPs have found vast applications in biomedical imaging, biomolecular processes, biosensing, and drug delivery, as well as for fabricating new bio-inspired materials. These applications hinge on the electrostatic and/or hydrophobic interactions of properly decorated Au NPs with biological molecules. [1-2]

Though the molecular recognition property of Au NPs could be tuned by choosing proper monolayer terminal groups, [3] one could find very few literature reports describing molecular level properties of the NPs' interfacial region, such as surface electrostatics and a gradient of local dielectric constant across the interface. Measuring and understanding these fundamental biophysical parameters at the NPs' interface will open new opportunities in biological and biomedical applications. The goal of our research is to combine advances of modern nanotechnology, organic synthesis and EPR spectroscopy and to develop spin probe EPR methods to assess dynamics and electrostatic and dielectric properties of the nanoparticle-biomolecule interfaces. The first step in this project is a preparation of small Au NPs coated with ionizable functional groups so the electrostatic properties of NPs can be adjusted and studied as a function of pH.

Two methods were employed to synthesize water-soluble Au NPs. First, we tried the two-phase synthesis method, which was introduced by Mathias Brust in 1994. [5] In this method, a solution of octanethiol (**4**) in toluene was added to aqueous hydrochloroauric acid. The two reactants formed an intermediate at the toluene/water

interface. The intermediate was reduced by sodium borohydride to yield the Au NPs. Using this method we successfully synthesized **4**-coated Au NPs with diameters around 0.5 nm. **4**-coated Au NPs are hydrophobic, but we wanted our Au NPs to be water-soluble. To prepare water-soluble NPs, we synthesized a ligand with charged terminal amino groups - 11-(dimethylamino)undecane-1-thiol hydrochloride (**5**) [6] and tried to replace **4** with **5** through the ligand-exchange reaction. [7] [8] However, due to the low ligand exchange efficiency and nanoparticles aggregations caused by the long chain of ligands during the reaction, [9] we had to give up this method and tried to find a way to directly coat **5** onto Au NPs.

The second approach we applied is based on the one-pot synthesis method, [10] [11] which is widely used in recent years. We utilized a mixture of THF and acetic acid as the solvent instead of pure THF mentioned in literature.

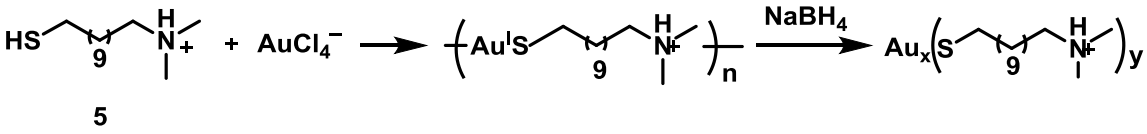

Fig. 1.7 Scheme of the synthesis of 11-(dimethylamino)undecane-1-thiol hydrochloride-coated water soluble Au NPs.

5 and hydrochloroauric acid were co-dissolved in this solvent to form an intermediate. Then the intermediate was reduced by sodium borohydride and developed into water-soluble Au NPs. [12] The average diameter of these Au NPs were found to be around 1.5 nm by DLS and TEM. NP diameters from 0.5 to 2.0 nm are considered to be optimal in application to bio systems and biorecognition studies.

CHAPTER 2 RESULTS AND DISCUSSION

2.1 Ligands

Ligands with long hydrophobic carbon chains were synthesized and employed in our project. Some of them were used in the synthesis of Au NPs in order to make NPs ionizable so that NPs would be stable and monodispersed in different pH conditions. Other ligands were connected to nitroxides before coating to Au NPs. Such spin-labeled ligands are EPR active and could act as probes to detect local electrostatic properties of Au NPs.

2.1.1 Octanethiol (**4**)

Octanethiol is commercially available.

Octanethiol-coated Au NPs have hydrophobic properties, and are able to act as precursor towards water soluble Au NPs through ligand exchange reaction. The structure of **4** is shown below in Fig. 2.1.

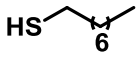

Fig. 2.1 Scheme of the structure of Octanethiol (4).

Octanethiol was used as a ligand to synthesize some hydrophobic Au NPs through two phase method. [5] This method was chosen because it is very mature and yielded highly stable Octanethiol-coated Au NPs with small (around 0.5 nm) diameter.

Our initial approach was to obtain some water soluble Au NPs by conducting ligand exchange experiment [7] [8] using Octanethiol-coated Au NPs and another ligand containing ionizable terminal group. Even though we did obtain some water soluble NPs, the average size of NPs increased and some of Au NPs aggregated in the

process of the ligand exchange. [9] Thus, we had no choice but abandon this approach and tried an alternative procedure to directly synthesize water soluble Au NPs.

2.1.2 11-(dimethylamino)undecane-1-thiol hydrochloride (5)

11-(dimethylamino)undecane-1-thiol hydrochloride contains an ionizable functional group so once decorated on Au NPs, it can make Au NPs more hydrophilic, and the electrostatic properties of NPs can be adjusted and studied as a function of pH. The structure of the ligand is shown below in Fig. 2.2.

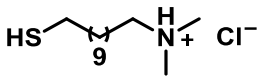

Fig. 2.2 Scheme of structure of 11-(dimethylamino)undecane-1-thiol hydrochloride (5).

5 was synthesized in three steps according to the literature protocol. [6] Firstly, 11-bromo-1-undecene was reacted with thioacetic acid in the presence of AIBN, resulting in thioacetic acid-S-(11-bromoundecyl) ester. [6a] We verified thioacetic acid-S-(11-bromoundecyl) ester by ^{1}H NMR (400 MHz, $CDCl_3$, δ). Secondly, dimethylamine reacted with thioacetic acid-S-(11-bromoundecyl) ester, [6b] and thirdly the resulting product was taken up in 20% solution of gaseous HCl in THF to form **5**. [6b] ^{1}H NMR (400 MHz, CD_3OD, δ) and IR were applied to characterize **5**.

2.1.3 11-Mercapto-1-undecanol (**6**)

6 was commercially purchased. The structure of **6** is shown in Fig. 2.3.

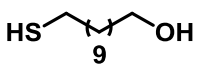

Fig. 2.3 Scheme of structure of 11-Mercapto-1-undecanol (6).

Compound **6** was used in two ways. Firstly, it was employed in ligand-exchange reaction in order to attach radicals to Au NPs. We tried to synthesize some Au NPs coated with both **5** and **6**, and then attach nitroxide radicals to **6** by a coupling reaction of OH group on **6** and COOH group on nitroxide radicals. However, the resulting Au NPs were EPR silent. This could be attributed to the low coverage of **6** on Au NPs. Alternatively, the long chain of **5** could produce steric problem for nitroxide radicals to get close to the OH group of **6**.

Secondly, compound **6** could also acts as a precursor of a disufide derivative, which will be described in 2.1.4 and later chapters.

2.1.4 11, 11'-Dithiodiundecanol (**7**)

The structure of this compound is shown in Fig. 2.4.

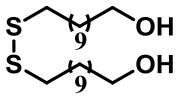

Fig. 2.4 Scheme of structure of11, 11'-Dithiodiundecanol (7).

7 was synthesized from **6** by an oxidation reaction with DMSO [13] or I_2, [14] and characterized by ^{1}H NMR (400 MHz, $CDCl_3$, δ).

We were able to attach nitroxide radical to **7** through DCC-mediated coupling reaction [15] of its OH groups and COOH group of nitroxide radical, as a result, we obtained a spin-labeled ligand. Then, the spin-labeled ligand was employed in ligand exchange experiments to obtain spin-labeled Au NPs.

Details of these experiments will be provided in later chapters.

2.1.5 12-(Acetylthio)dodecanol (**8**)

The structure of **8** is shown in Fig. 2.5.

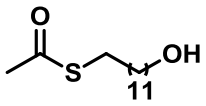

Fig. 2.5 Scheme of structure of 12-(Acetylthio)dodecanol (8).

8 was synthesized by a ssubstitution reaction of 11-Mercapto-1-dodecanol and Potassium thioacetate, [16] and characterized by ^{1}H NMR (400 MHz, $CDCl_3$, δ). We were able to attach nitroxide radical to this compound through coupling reaction to obtain a spin-labeled ligand. Then, the spin-labeled ligand was employed in ligand exchange to obtain spin-labeled Au NPs.

Details of these experiments will be provided in later chapters.

2.1.6 10-(Acetylthio)decanoic acid (**9**)

The structure of ths compound is shown in Fig. 2.6

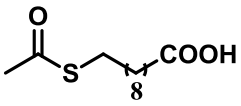

Fig. 2.6 Scheme of the structure of 10-(Acetylthio)decanoic acid (9).

This ligand was synthesized by a ssubstitution reaction of 10-bromodecanoic acid and Potassium thioacetate, [16] and verified by ^{1}H NMR (300 MHz, $CDCl_3$, δ). It was successfully coupled with nitroxide radical to form a spin-labeled ligand and then employed in ligand exchange experiments.

Details of these experiments will be provided in later chapters.

2.2 Nitroxide Radicals

2.2.1 3-Carboxy-2,2,5,5-tetramethyl-3-pyrroline-1-oxyl (**1**)

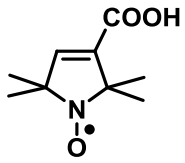

Fig. 2.7 Scheme of the structure of 3-Carboxy-2,2,5,5-tetramethyl-3-pyrroline-1-oxyl (1).

1 was purchased from a commercial source. This radical was employed to study the dynamics of the self-assembled monolayers. We were able to attach OH group containing ligands to **1** to form spin-labeled ligands. **1** is not intrinsically sensitive to the pH of the medium since it does not contain an ionizable group.

2.2.2 2-(2-Carboxyethyl)-2,3,4,5,5-pentamethylimidazolidine-1-oxyl (**2**)

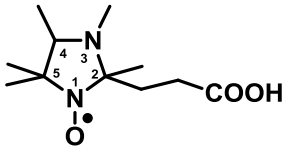

Fig. 2.8 Scheme of the structure of 2-(2-Carboxyethyl)-2,3,4,5,5-pentamethylimidazolidine-1-oxyl (2)

2 is pH-sensitive nitroxide since it has a nitrogen atom at position 3, which could be protonated or nonprotonated in different environment. When attached to other ligands, **2** could act as a pH-sensitive spin probe: its protonated and non-protonated forms are

expected to have different isotropic nitrogen hyperfine splittings that could be measured from EPR spectra. [17] Based on the change in isotropic hyperfine splittings we were able to determine the pK_a of these spin-labeled ligands. After coating such spin-labeled ligands onto Au NPs, interfacial pK_a of the resulting spin-labeled Au NPs could be measured.

2 was synthesized through five steps, [18] as shown in Fig. 2.9.

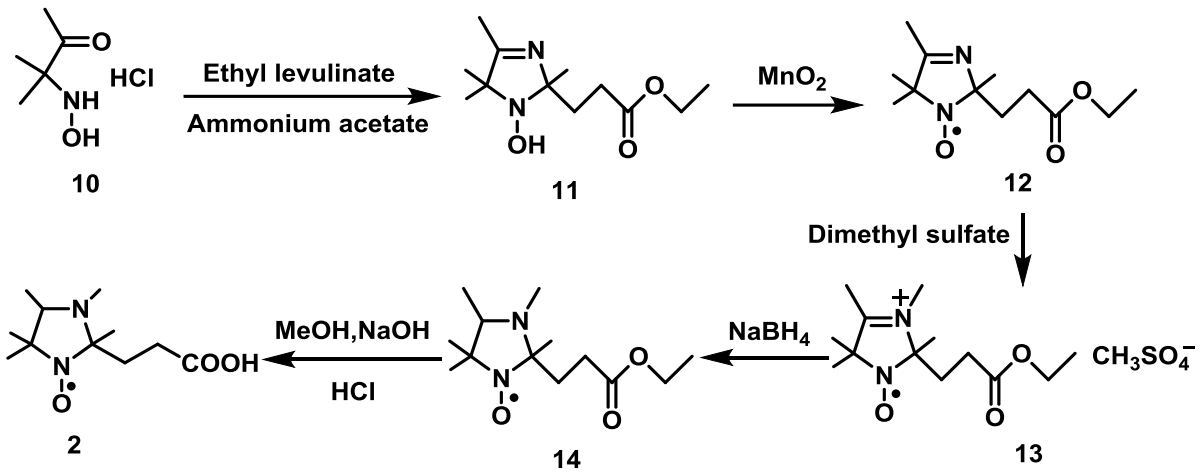

Fig. 2.9 Scheme of synthesis of 2-(2-Carboxyethyl)-2,3,4,5,5-pentamethylimidazolidine-1-oxyl (2)

Firstly, the corresponding 1-hydroxy-3-imidazoline derivative (**11**, Fig. 2.3) was formed by slowly refluxing hydroxyamino ketone (**10**, Fig. 2.3) in methanol in the presence of ammonium acetate. Secondly, **11** was oxidized by MnO_2 in chloroform to form the corresponding radical (**12**, Fig. 2.3). Thirdly, 2-(2-methoxycarbonylethyl)-2,3,4,5,5-pentamethyl-3-imidazolinium 1-oxyl methylsulfate (**13**, Fig. 2.3) was formed by mixing **12** and dimethyl sulfate in try ether. Fourthly, **13** was reduced by sodium borohydride to form 2-(2-methoxycarbonylethyl)-2,3,4,5,5-pentamethylimidazolidine 1-oxyl (**14**, Fig. 2.3). Finally, **14** was hydrolyzed into **2**.

The success of this 5-step process was verified by characterization **14** with IR and Mass Spec and **2** with IR.

2.2.3 4-(2-Aminoethylamino)-1-oxyl-2,2,5,5-tetramethyl-2,5-dihydro-1H-imidazole (**3**)

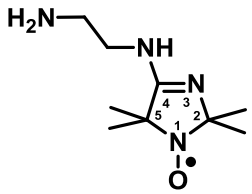

Fig. 2.10 Scheme of structure of 4-(2-Aminoethylamino)-1-oxyl-2,2,5,5-tetramethyl-2,5-dihydro-1H-imidazole (3).

3 was provided by Dr. Maxim A. Voinov in our group.

3 has a nitrogen atom at position 3 as well as two amino groups on its side chain. As a result, the nitrogen atom at position 3 and the two amino groups on its side chain are all ionizable and could be protonated or nonprotonated in different environment.

3 could act as a pH-sensitive spin probe: its protonated and non-protonated forms are expected to have different isotropic nitrogen hyperfine splittings that could be measured from EPR spectra. Based on the change in isotropic hyperfine splittings we were able to determine the pK_a of these spin-labeled ligands. After coating such spin-labeled ligands onto Au NPs, interfacial pK_a of the resulting spin-labeled Au NPs could be measured.

2.3 Spin-labeled Ligands

Spin-labeled ligands were obtained through DCC-mediated coupling reactions[15] of ligands and nitroxide radicals. The ligands were introduced into the ligand layer of Au NPs through ligand exchange experiments, so that they could act as probes to detect local environment of Au NPs.

Structures of nitroxide-modified disulfide and thioacetyl ligands used in this project are shown in the Fig. 2.11. The details of the synthesis of the nitroxides and the spin-labeled ligands are discussed further in this Chapter and in the Experimental Part.

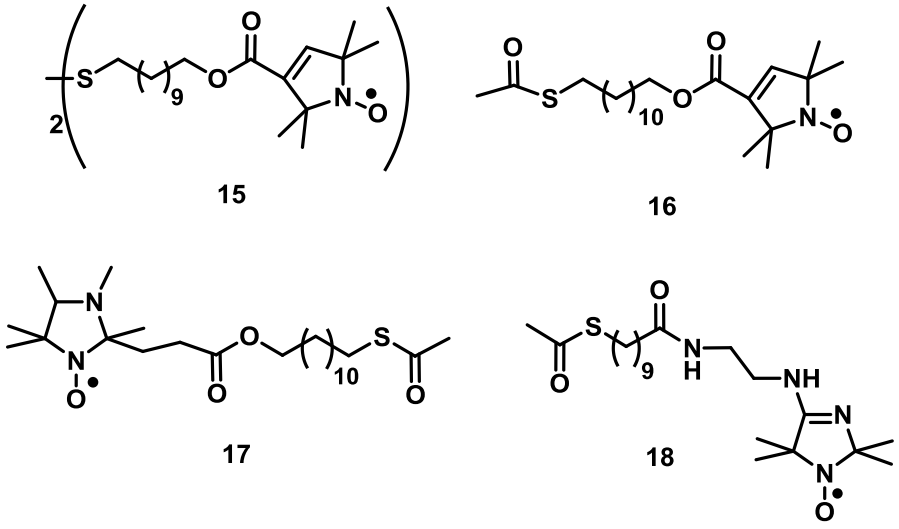

Fig. 2.11 Scheme of chemical structures of spin-labeled ligands used in this project. 15: 1,2-bis(undecyl 1-oxyl-2,2,5,5-tetramethyl-2,5-dihydro-1H-pyrrole-3-carboxylate)disulfide, 16: 12-(acetylthio)dodecyl 1-oxyl-2,2,5,5-tetramethyl-2,5-dihydro-1H-pyrrole-3-carboxylate, 17: 12-(acetylthio)dodecyl 3-(3-oxyl-1,2,4,4,5-pentamethylimidazolidin-2-yl)propanoate, 18: S-10-oxo-10-(2-(1-oxyl-2,2,5,5-tetramethyl-2,5-dihydro-1H-imidazol-4-ylamino)ethylamino)decyl ethanethioate.

2.3.1 1,2-bis(undecyl 1-oxyl-2,2,5,5-tetramethyl-2,5-dihydro-1H-pyrrole-3-carboxylate) disulfide (**15**)

15 was synthesized through coupling reaction of **7** and **1**. [15]The reaction formula is shown in Fig. 2.12.

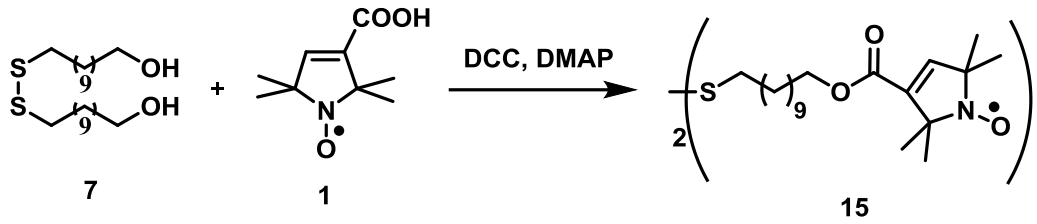

Fig. 2.12 Scheme of the synthesis of 1,2-bis(undecyl 1-oxyl-2,2,5,5-tetramethyl-2,5-dihydro-1H-pyrrole-3-carboxylate) disulfide (15).

15 was verified by IR spectrum. **15** could be coated to Au NPs through ligand exchange experiment with **5**-coated Au NPs, resulting in Au NPs partially coated by **15**. Such **15**-coated Au NPs were EPR active. We chose to use **15** because it was reported that disulfide nitroxides could be attached to Au NPs through ligand exchange experiment. [19] However, due to the steric problem caused by the long carbon chain of **5**, the efficiency of ligand exchange experiment was rather low. Although we were able to collect some EPR spectra, the peak intensities were extremely low. We will follow **15**-coated Au NPs later in this chapter as well as in other chapters.

2.3.2 12-(acetylthio)dodecyl 1-oxyl-2,2,5,5-tetramethyl-2,5-dihydro-1H-pyrrole-3-carboxylate (**16**)

16 was synthesized through coupling reaction of **8** and **1**. [15] The reaction formula is shown in Fig. 2.13.

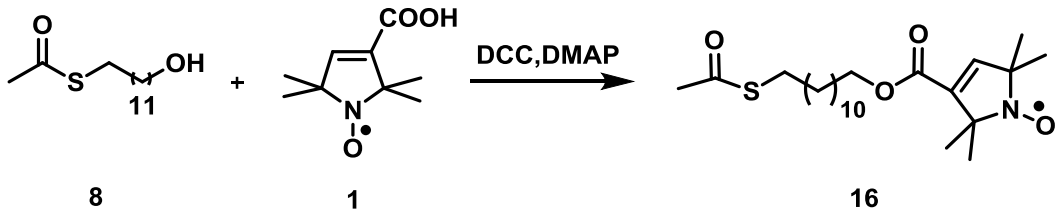

Fig. 2.13 Scheme of the synthesis of 12-(acetylthio)dodecyl 1-oxyl-2,2,5,5-tetramethyl-2,5-dihydro-1H-pyrrole-3-carboxylate (16).

16 was verified by IR spectrum. **16** was coated to Au NPs through ligand exchange experiment with **5**-coated Au NPs, resulting in Au NPs partially coated by **16**. Since **8** has a longer carbon chain than **5**, the radical group of **16** was able to stretch out and was detected by EPR. Besides, **16** is more sterically favorable than **15** in the ligand exchange experiment. As a result, **16**-coated Au NPs produced informative EPR spectra that will be described in details later in this chapter.

2.3.3 12-(acetylthio)dodecyl 3-(3-oxyl-1,2,4,4,5-pentamethylimidazolidin-2-yl)propanoate (**17**)

17 was synthesized through coupling reaction of **8** and **2**. [15] The reaction formula is shown in Fig. 2.14.

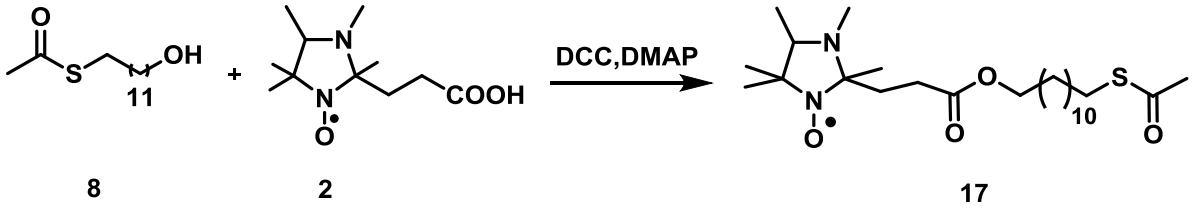

Fig. 2.14 Scheme of the synthesis of 12-(acetylthio)dodecyl 3-(3-oxyl-1,2,4,4,5-pentamethylimidazolidin-2-yl)propanoate (17).

17 was verified by IR spectrum and Mass Spectroscopy. **17** was coated to Au NPs through ligand exchange experiment with **5**-coated Au NPs, resulting in Au NPs partially coated by **17**. Since **17** is similar to **16** ligand, **17** also yielded informative EPR spectra. It os important to note here is that **17** is pH-sensitive due to ionizable property of **2**, thus, **17**-coated Au NPs were also pH-sensitive and were able to act as probes to detect local electrostatic environment.

However, according to our pH-titrating result (later in this chapter), pK_a of **17** in bulk water is 3.28. Our aim is to apply spin-labeled Au NPs in biosystems, which have relatively neutral pH. In such neutral environment **17**-labeled Au NPs would be completely nonprotonated, making it silent to any slight change in local electrostatic environment which we are interested in. So we had to find out another spin-labeled ligand with higher pK_a value.

2.3.4 S-10-oxo-10-(2-(1-oxyl-2,2,5,5-tetramethyl-2,5-dihydro-1H-imidazol-4-ylamino)ethylamino)decyl ethanethioate (**18**)

18 was synthesized through coupling reaction of **9** and **3**. [15]The reaction formula is shown in Fig. 2.15.

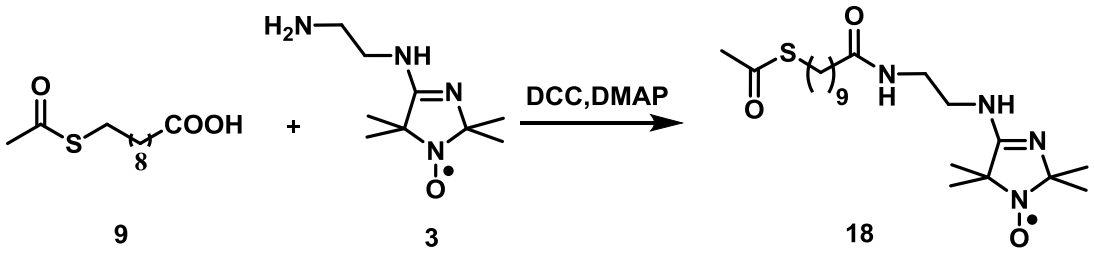

Fig. 2.15 Scheme of the synthesis of S-10-oxo-10-(2-(1-oxyl-2,2,5,5-tetramethyl-2,5-dihydro-1H-imidazol-4-ylamino)ethylamino)decyl ethanethioate (18).

18 was verified by IR spectrum and Mass Spectroscopy. **18** was coated to Au NPs through ligand exchange experiment with **5**-coated Au NPs, resulting in Au NPs partially coated by **18**. Since **18** also contains a long chain, it also produced informative EPR spectra. More importantly, due to the ionizable properties of nitrogen atom at position 3 of **3** and the two amino groups on its side chain, **18** was expected to be of a higher pK_a than **17**. This assumption was verified in pH-titration experiment using compand **18** that will be described later in this chapter.

2.4 Au NPs

2.4.1 11-(dimethylamino)undecane-1-thiol hydrochloride-coated water soluble Au NP (**19**)

19 was synthesized using a slightly modified procedure of Dr. Victor Chechik (Fig. 2.16).[20] Tetrachloroaurate and **5** were vigorously stirred in a mixture of THF and acetic acid (THF/acetic acid = 6) at room temperature overnight to form an intermediate and then cooled to 0 ^{0}C. Ice-cold sodium borohydride aqueous solution was added quickly to the ice-cold reaction mixture and vigorously stirred at 0 ^{o}C for another 24 hrs to form stable Au NPs of small sizes.

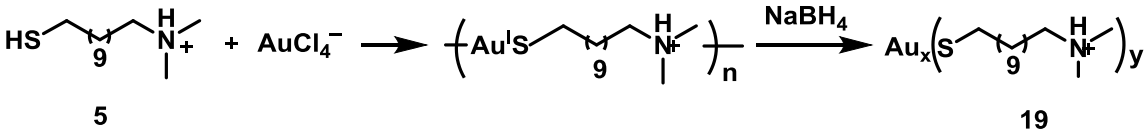

5 19

Fig. 2.16 Scheme of the synthesis of 11-(dimethylamino)undecane-1-thiol hydrochloride-coated water soluble Au NP (19).

The average diameter of **19** was measured by TEM and DLS, as shown in Fig. 2.17 and 2.18.

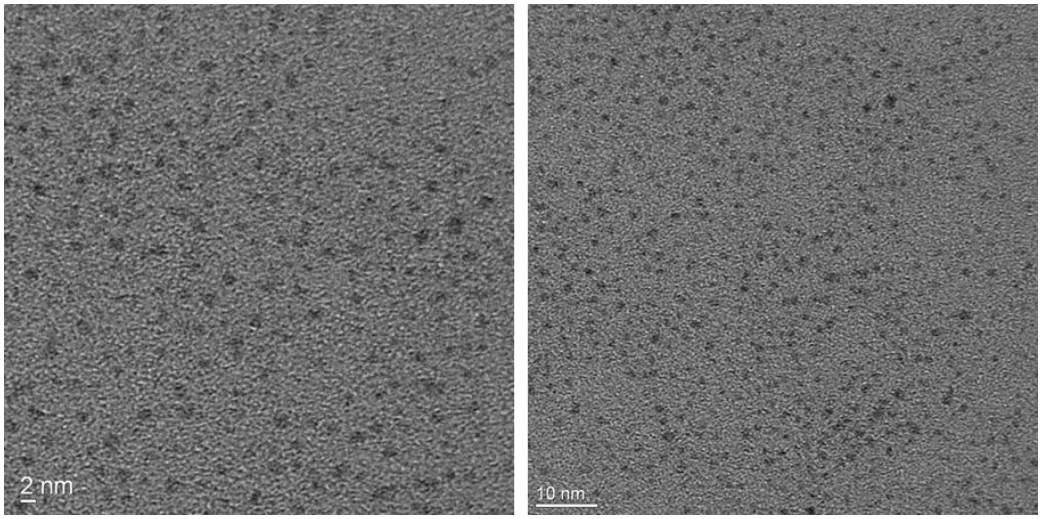

Fig. 2.17 TEM images of Au NPs.

Both of them came from the same freshly synthesized 19. The one on the left has a ruler of 2nm while the right one has a ruler of 10nm.

Table 2.1 Statistics of DLS data for size measurement of 11-(dimethylamino)undecane-1-thiol hydrochloride-coated water soluble Au NP from the same freshly prepared sample

Size	Mean	Std Dev		Size	Mean	Std Dev		Size	Mean	Std Dev		Size	Mean	Std Dev
d.nm	Number %	Number %		d.nm	Number %	Number %		d.nm	Number %	Number %		d.nm	Number %	Number %
0.4	0			5.615	0			78.82	0			1106	0	
0.4632	0			6.503	0			91.28	0			1281	0	
0.5365	0			7.531	0			105.7	0			1484	0	
0.6213	0			8.721	0			122.4	0			1718	0	
0.7195	0			10.1	0			141.8	0			1990	0	
0.8332	0			11.7	0			164.2	0			2305	0	
0.9649	4		3.8596	13.54	0			190.1	0			2669	0	
1.117	15.9		17.7603	15.69	0			220.2	0			3091	0	
1.294	26.3		34.0322	18.17	0			255	0			3580	0	
1.499	24.8		37.1752	21.04	0			295.3	0			4145	0	
1.736	16		27.776	24.36	0			342	0			4801	0	
2.01	8.1		16.281	28.21	0			396.1	0			5560	0	
2.328	3.4		7.9152	32.67	0			458.7	0			6439	0	
2.696	1.2		3.2352	37.84	0			531.2	0			7456	0	
3.122	0.4		1.2488	43.82	0			615.1	0			8635	0	
3.615	0.1		0.3615	50.75	0			712.4	0			1.00E+04	0	
4.187	0			58.77	0			825	0					
4.849	0			68.06	0			955.4	0					

Table 2.1 contitued

Size	Mean	Std Dev		Size	Mean	Std Dev		Size	Mean	Std Dev		Size	Mean	Std Dev
d.nm	Volume %	Volume %		d.nm	Volume %	Volume %		d.nm	Volume %	Volume %		d.nm	Volume %	Volume %
0.4	0			5.615	0			78.82	0			1106	0	
0.4632	0			6.503	0			91.28	0			1281	0	
0.5365	0			7.531	0.1			105.7	0			1484	0	
0.6213	0			8.721	0.1			122.4	0			1718	0	
0.7195	0			10.1	0.1			141.8	0			1990	0	
0.8332	0			11.7	0.1			164.2	0			2305	0	
0.9649	1.5			13.54	0.1			190.1	0			2669	0	
1.117	7.4			15.69	0.1			220.2	0			3091	0	
1.294	16.2			18.17	0.1			255	0			3580	0	
1.499	21.2			21.04	0.1			295.3	0			4145	0	
1.736	20			24.36	0.1			342	0			4801	0	
2.01	15			28.21	0			396.1	0			5560	0	
2.328	9.4			32.67	0			458.7	0			6439	0	
2.696	5			37.84	0			531.2	0			7456	0	
3.122	2.2			43.82	0			615.1	0			8635	0	
3.615	0.8			50.75	0			712.4	0			1.00E+04	0	
4.187	0.2			58.77	0			825	0					
4.849	0			68.06	0			955.4	0					

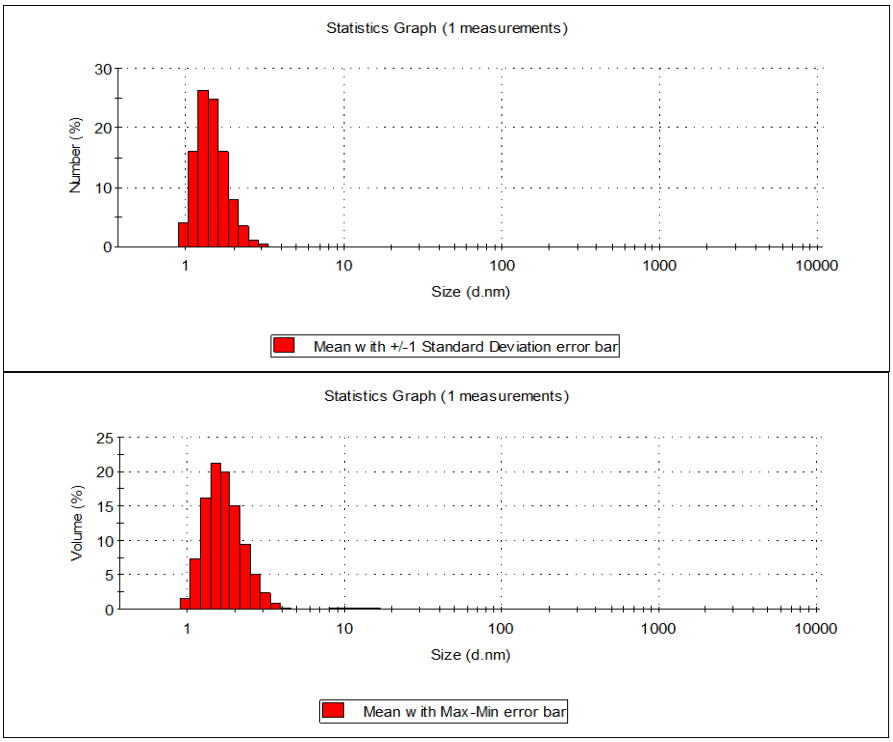

Fig. 2.18 DLS analysis of the nanoparticle solution from the same sample of 11-(dimethylamino)undecane-1-thiol hydrochloride-coated water soluble Au NP (19) freshly prepared. These graphs were generated based on the corresponding data from table 2.1.

From TEM and DLS results we can conclude that the average diameter of Au NPs is 1.49 nm. From TEM, we can visually see that NPs were roughly of similar sizes around 2 nm (Fig. 2.17). And DLS (Fig. 2.18) provides statistics data (Table 2.1) from which we were able to calculate the average size of Au NPs to be 1.49 nm:

$$Size = \frac{\sum_{i=1}^{n} Size_i \times MeanNumber\%_i}{100\%} \quad (2.1)$$

We did not use the mean volume to do the calculation because there were some large sizes of pretty small percentages in its statistics data. These data may be attributed to dusts in solution since there sizes were not close to that of Au NPs if we compare the TEM images and DLS graphs. Besides, from DLS graph based on mean number% we can also see that the number of such dusts was too low to be counted in.

The extent of the nanoparticle surface coating was determined using thermogravimetric analysis (TGA) (Fig. 2.19). In the TGA graph, **19** were stable when heated from room temperature to 200 ^{0}C, followed by mass loss from 200 ^{0}C to 500 ^{0}C and then the weight of residue was stable with increasing temperature. We attributed the mass loss between 200^{0}C and 500^{0}C to the loss of **5**, so this mass loss should be the mass of **5** coating on Au NPs. The weight of residue was the mass of Au cores (table in Fig. 2.19). As a result, we could calculate the moles of **5** and Au atom in this TGA sample separately.

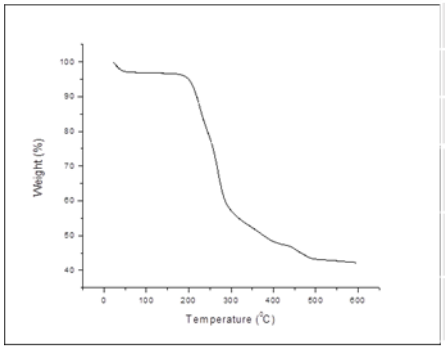

Temperature (℃)	weight (mg)	weight (%)
200	4.49	94.96
293	2.76	58.36

Weight of ligand (mg)	weight of Au (mg)
1.73	2.04
0.00648 mmol	0.0104 mmol

Fig. 2.19 Results of the TGA analysis of 11-(dimethylamino)undecane-1-thiol hydrochloride-coated water soluble Au NP (19).

Using a combination of the results from the nanoparticle size measurement and the thermogravimetric analysis, the composition of **19** was estimated as follows.

Given that the diameter of Au NPs is 1.49 nm (based on DLS analysis), the volume of each Au nanocore is

$$\mathrm{V_{NP}} = \frac{4}{3}\pi \mathrm{r}^3 = \frac{4}{3}\pi(\frac{14.9}{2})^3 = 173\ \text{Å}^3 = 1.73 \times 10^{-27} m^3 = 1.73 \times 10^{-21} cm^3 \qquad (2.2)$$

The volume of Au cubic unit cell is

$$\mathrm{V_{Au\ cubic\ unit}} = l^3 = (4.0786\text{Å})^3 = 67.847\text{Å}^3 \qquad (2.3)$$

The density of gold is 19.3 g/cm^3, so mass of gold nanocore = 3.34× 10^{-20}g.

So number of gold atoms in nanoparticle is

$$\frac{\text{mass}}{197\text{g/mol}} \times \mathrm{N_A} = \frac{3.34\times10^{-20}\text{g}}{197\text{g/mol}} \times 6.022 \times 10^{23}/\mathrm{mol} = 102 \text{ atoms per nanoparticle} \qquad (2.4)$$

Surface area of NP sphere

$$\mathrm{S}=4\pi \mathrm{r}^2 = 4\pi\left(\frac{14.9\text{Å}}{2}\right)^2 = 697.5\text{Å}^2 \qquad (2.5)$$

According to ref [21], the average length of Au-Au bond on surface of Au NP is 2.93 $\mathring{A}$. If we use a lattice model to mimic the gold arrangement on surface, the number of Au atom in each cell is 1. Number of cells on the surface= $\frac{S}{2.93^2} \approx 81$ cells. As a result, 21 atoms are in the core while 81 atoms on the surface.

From TGA data, sample containing 1.0358×10^{-5} mol Au atoms also contains 6.48×10^{-6} mol ligands (266.5 g/mol) (We consider the weight loss from 200℃ to 293℃ as the loss of ligands). So the amount of Au NPs in TGA sample is

$$\text{Au NPs} = \frac{1.0358 \times 10^{-5}}{102} = 1.02 \times 10^{-7}\text{mol} \quad (2.6)$$

The amount of ligands in each Au NP is

$$\frac{\text{Ligand}}{\text{NPs}} = (6.48 \times 10^{-6}\text{mol})/(1.02 \times 10^{-7}\text{mol}) = 63\ ligands/\text{NP} \quad (2.7)$$

Thus, the composition of **19** we have synthesized is estimated to be $Au_{102}ligand_{63}$. This estimated composition is very close to the reported Au NP composition [22], $Au_{144}ligand_{60}$, the size of which is also close to the NPs synthesized by us. Besides, the model applied in our estimation results in less Au atoms in the nanocore, since Au atoms are reported [23] to pack more tightly than natural Au which has a density of 19.3 g/cm^3. So it is reasonable to think that there should be more than 102 Au atoms per NP. As a result, we assume that the composition of Au NPs we obtained is $Au_{144}ligand_{60}$.

The stability of **19** was characterized by zeta potential as a function of pH, [24] which is shown in Fig. 2.20.

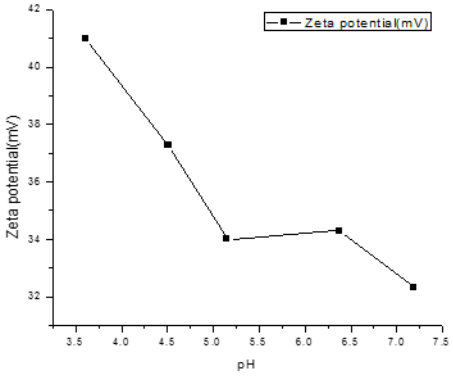

pH	Zeta Potential (mV)
3.61	41
4.51	37.3
5.15	34
6.38	34.3
7.19	32.3

Fig. 2.20 Zeta potential of 11-(dimethylamino)undecane-1-thiol hydrochloride-coated water soluble Au NP (19) in ultra-pure water. The pH of each data point was adjusted by 0.02 M HCl solution and 0.02 M NaOH solution.

When the pH goes up, the zeta potential goes down. This demonstrates that **19** is most stable under acetic conditions, which coincides with our expectation, since the amino groups would better stabilize NPs by repulsion while more of them are positively charged. [25]

2.4.2 1,2-bis(undecyl 1-oxyl-2,2,5,5-tetramethyl-2,5-dihydro-1H-pyrrole-3-carboxylate) disulfide-modified Au NPs (**20**)

15 was coated to Au NPs surface through ligand exchange experiment (Fig. 2.21). [20]

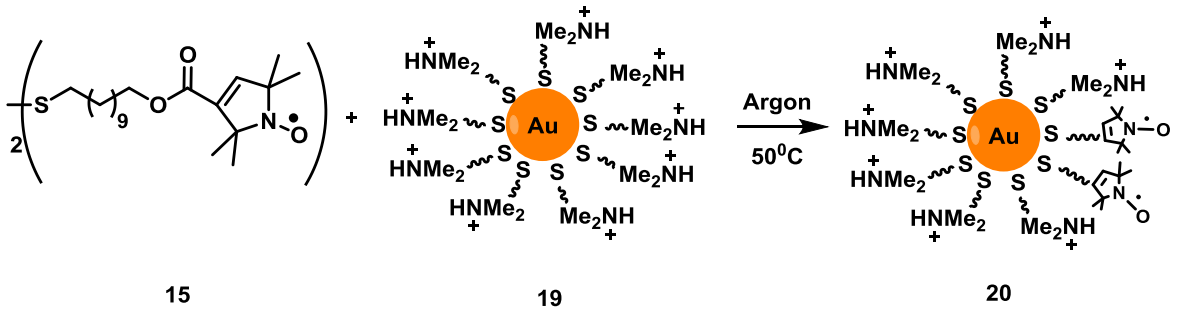

Fig. 2.21 Scheme of the synthesis of 1,2-bis(undecyl 1-oxyl-2,2,5,5-tetramethyl-2,5-dihydro-1H-pyrrole-3-carboxylate) disulfide-modified Au NPs (20).

Ligand exchange experiments were conducted with **15** : Au NP =5:1,10:1, and 20:1. We purified each **15**-modified NPs sample and collected X-band (9.5 GHz) EPR spectra as shown in Fig. 2.22.

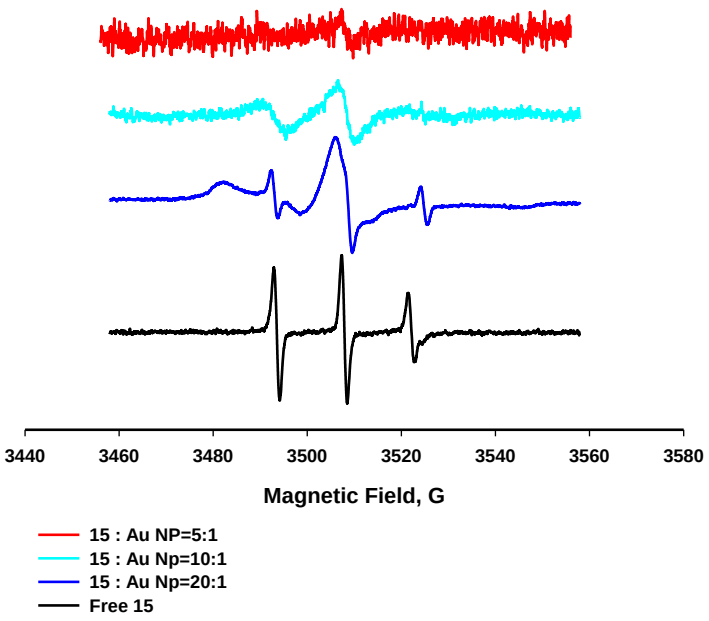

Fig. 2.22 EPR spectra acquired from samples of 1,2-bis(undecyl 1-oxyl-2,2,5,5-tetramethyl-2,5-dihydro-1H-pyrrole-3-carboxylate) disulfide-modified Au NPs ligand exchanged at various 15/NP ratios.

As is shown above, the EPR signals of **20** are weak. Only those ligand exchanged with highest **15**/NP ratio (**15** : NP = 20:1) have relatively strong EPR signal with low noise. However, NPs of this **15**/NP ratio were easily aggregated in water since the high percentage of **15** coating on NP surface highly weakened the repulsion created by **5** between NPs. As a result, we were in need of a different kind of spin-labeled ligand which has longer chain than **5** and better accessibility to surface of NP than **15** so that nitroxide radical on the tail of **15** could be easily detected by EPR other than buried by **5**.

2.4.3 12-(acetylthio)dodecyl 1-oxyl-2,2,5,5-tetramethyl-2,5-dihydro-1H-pyrrole-3-carboxylate-modified Au NPs (**21**)

16 was attached to Au NPs surface through ligand exchange experiment (Fig. 2.13).

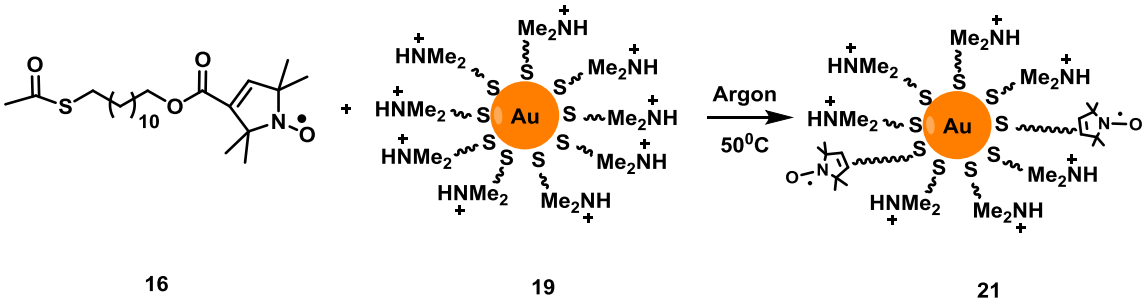

Fig. 2.23 Scheme of the synthesis of 12-(acetylthio)dodecyl 1-oxyl-2,2,5,5-tetramethyl-2,5-dihydro-1H-pyrrole-3-carboxylate-modified Au NPs (21).

Ligand exchange experiments were conducted with **16** : Au NP =10:1, 20:1, and 40:1. We purified each **21** sample and collected X-band (9.5 GHz) EPR spectra as shown in Fig. 2.24.

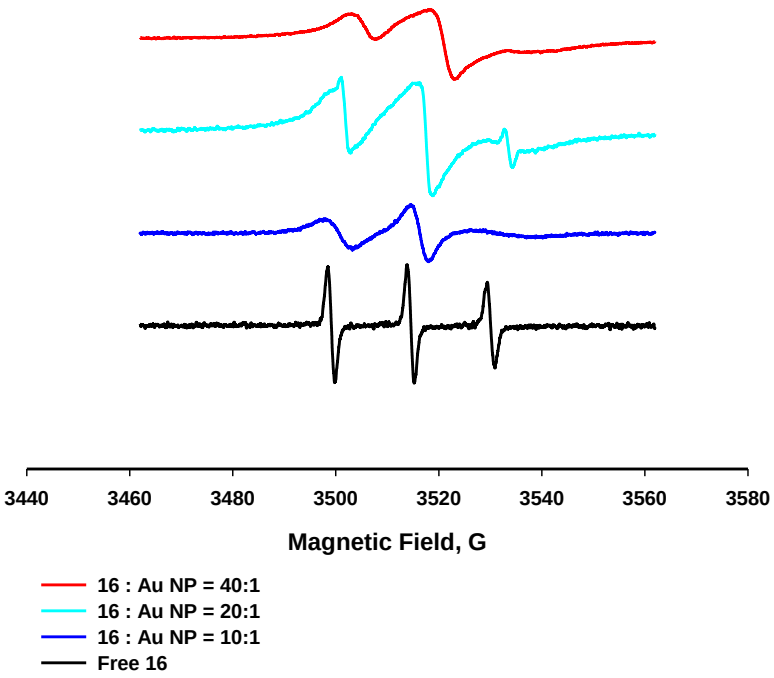

Fig. 2.24 EPR spectra acquired from 12-(acetylthio)dodecyl 1-oxyl-2,2,5,5-tetramethyl-2,5-dihydro-1H-pyrrole-3-carboxylate-modified Au NPs ligand exchanged at various 16/NP ratios.

As is shown above, the EPR signals of **21** have reasonable intensity with a low noise. When **16**/NP = 10:1, Au NPs have relatively noticeable EPR signal with low noise and little aggregation, while higher spin-labeled ligand ratios caused aggregation of NPs.

So the proper length of spin-labeled ligand should be a little bit longer than **5** in order to obtain satisfying EPR signals. So pH-sensitive spin-labeled ligands with proper ligand lengths could be used to coat NPs so that the electronic properties of local environment of Au NPs could be detected by EPR once NPs are coated by this kind of ligands.

2.4.4 12-(acetylthio)dodecyl 3-(3-oxyl-1,2,4,4,5-pentamethylimidazolidin-2-yl)propanoate-modified Au NPs (**22**)

17 was attached to Au NPs surface through ligand exchange experiment (Fig. 2.25).
[20]

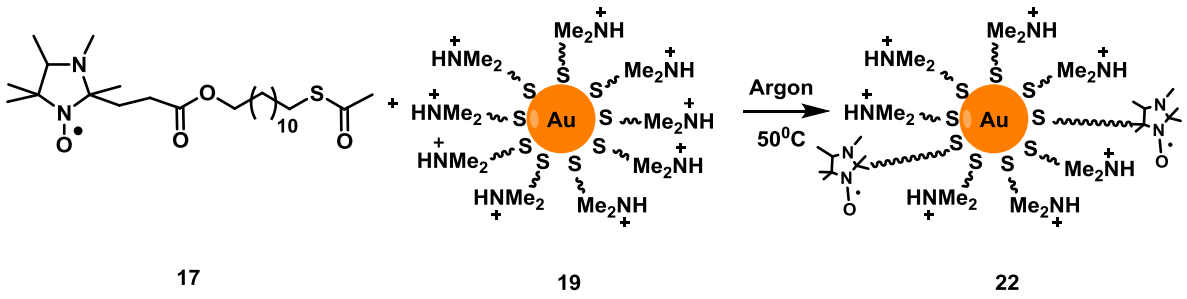

Fig. 2.25 Scheme of the synthesis of 12-(acetylthio)dodecyl 3-(3-oxyl-1,2,4,4,5-pentamethylimidazolidin-2-yl)propanoate-modified Au NPs (22).

Ligand exchange experiments were conducted with **17** : Au NP = 10:1. We purified **22** samples and collected X-band (9.5 GHz) EPR spectra in buffer solutions of different pH as shown in Fig. 2.26.

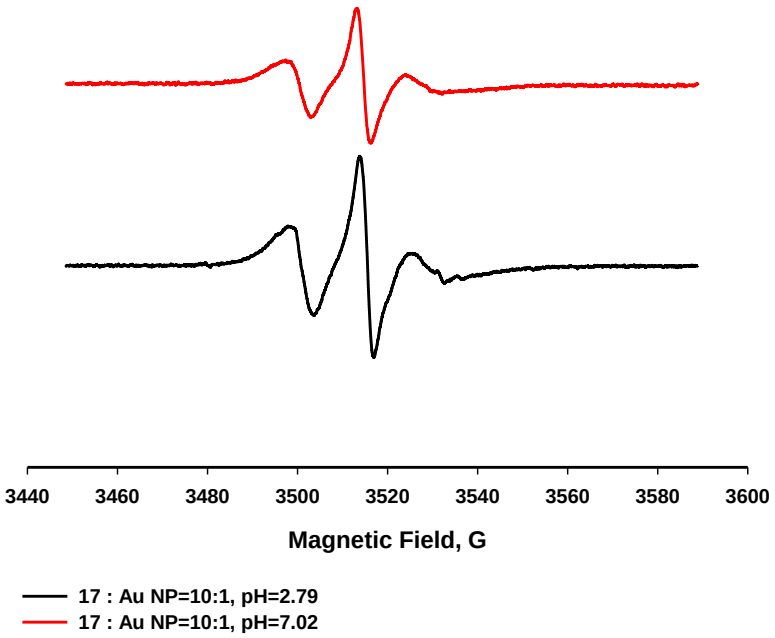

Fig. 2.26 EPR spectra of 12-(acetylthio)dodecyl 3-(3-oxyl-1,2,4,4,5-pentamethylimidazolidin-2-yl)propanoate-modified Au NPs under different pH conditions.

As shown above, the EPR spectra of Au NPs under different pH conditions are very similar in shape with each other, indicating that the local electro-dynamic environment does not change much under these pH conditions. This is because that the p*K*a (3.28) of **22** is even lower after attached to Au NPs so that even at acetic condition (pH=2.79) it is still nonprotonated.

2.4.5 S-10-oxo-10-(2-(1-oxyl-2,2,5,5-tetramethyl-2,5-dihydro-1H-imidazol-4-ylamino)ethylamino)decyl ethanethioate-modified Au NP (**23**)

18 was attached to Au NPs surface through ligand exchange experiment (Fig. 2.27).[20]

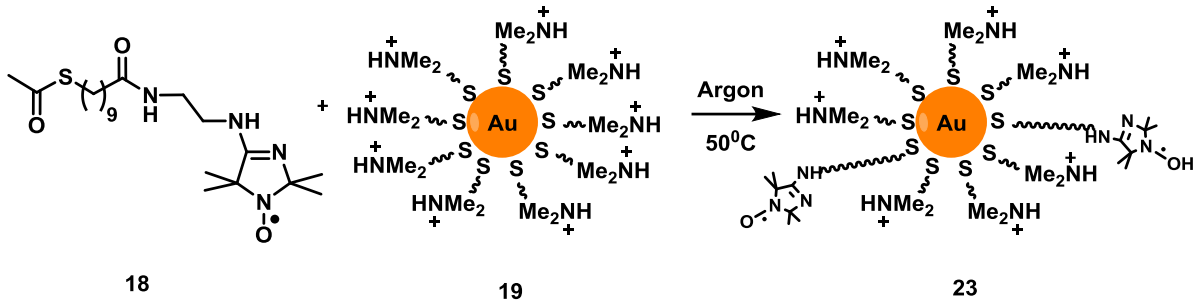

Fig. 2.27 Scheme of the synthesis of S-10-oxo-10-(2-(1-oxyl-2,2,5,5-tetramethyl-2,5-dihydro-1H-imidazol-4-ylamino)ethylamino)decyl ethanethioate-modified Au NP.

Ligand exchange experiments were conducted with **18** : Au NP = 40:1. We purified **23** samples and collected X-band (9.5 GHz) EPR spectra in SDS solutions (SDS/**5**, 4:1) of different pH as shown in Fig. 2.28.

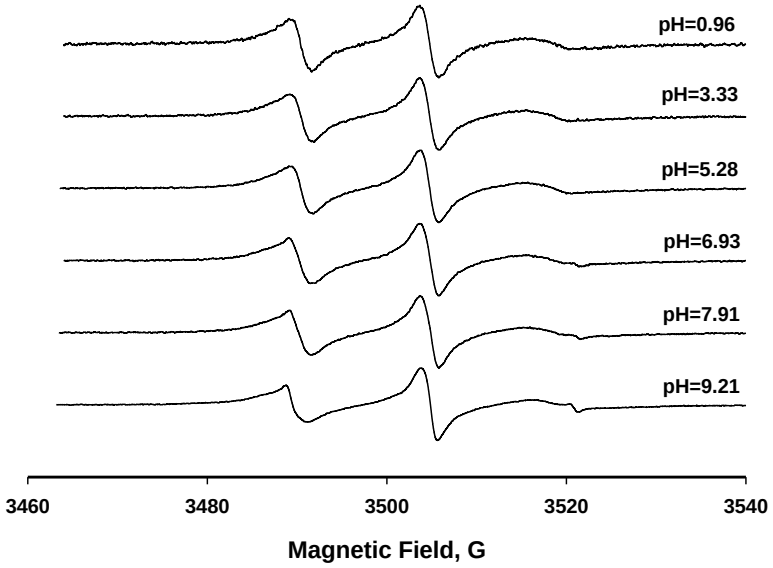

Fig. 2.28. Representative room-temperature X-band EPR spectra of S-10-oxo-10-(2-(1-oxyl-2,2,5,5-tetramethyl-2,5-dihydro-1H-imidazol-4-ylamino)ethylamino)decyl ethanethioate-modified Au NP taken at various pH in a series of aqueous solutions in the presence of SDS (SDS/5, 4:1). Solution pH of is indicated next to the corresponding spectra.

As shown above, shapes of EPR spectra of **23** changed according to pH, demonstrating the pH sensitivity of **23**. Details of this change will be further discussed in the titration part of this chapter.

SDS was used as charge compensation which has a relevance to biological application of NPs, because an interaction of NPs with such negatively charged polyelectrolytes as nucleic acids would result in a similar effect. SDS is mimicking the electrostatic properties of nucleic acids, providing a model environment for biological/biophysical applications of spin-labeled Au NPs. More advantages of applying SDS will be discussed in the titration part of this chapter.

As a result, **23** was successfully synthesized as pH sensitive Au NPs that has the potential to be applied to biosystems.

2.5 Titration of pH Sensitive Spin-labeled Ligands

It is expected that the intrinsic pK_a of the reported nitroxides will change for the terms corresponding to electrostatic and polarity contribution after the nitroxide-modified ligands were incorporated into the charged non-polar ensemble of NP-coating ligands: $\mathrm{p}K_a^i = \mathrm{p}K_a^0 + \Delta\mathrm{p}K_a^{el} + \Delta\mathrm{p}K_a^{pol}$, where $\mathrm{p}K_a^0$ is an intrinsic pK_a of the probe observed in pure water, and $\Delta\mathrm{p}K_a^{pol}$ and $\Delta\mathrm{p}K_a^{el}$ are electrostatic and polarity contributions, respectively.

Thus, to characterize the nitroxide-modified ligands we have synthesized, their intrinsic pK_a's (pK_a's in aqueous solution) have to be determined. However, these spin-labeled ligands are very hydrophobic and insoluble in water. In order to determine their pK_a's in bulk water, we pH-titrated these ligands in a series of buffer solution-isopropanol mixtures varying the concentration of isopropanol.[26,27] The experimental pK_a's acquired this way were extrapolated to 100% water.

2.5.1 12-(acetylthio)dodecyl 3-(3-oxyl-1,2,4,4,5-pentamethylimidazolidin-2-yl)propanoate (**17**).

An experimental X-band (9.5 GHz) EPR spectra of the nitroxide-modified ligand **17** taken in buffer solution-isopropanol mixtures at various pH are shown in Fig. 2.29.

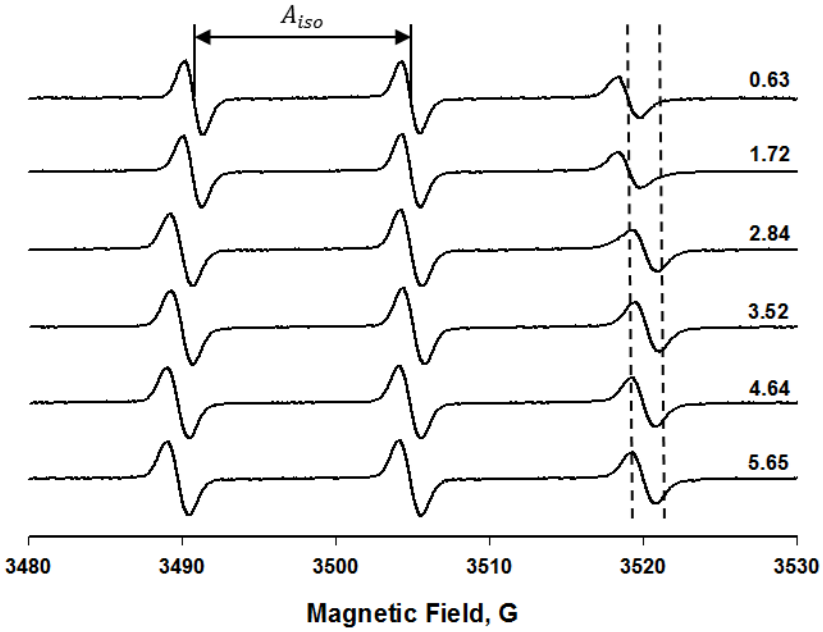

Fig. 2.29 Representative room-temperature X-band EPR spectra of 12-(acetylthio)dodecyl 3-(3-oxyl-1,2,4,4,5-pentamethylimidazolidin-2-yl)propanoate (17) in a series of buffer solutions containing 40% of isopropanol. pH of the solutions are indicated next to the corresponding spectra. Dashed lines mark approximate positions of the high-field nitrogen hyperfine coupling components corresponding to protonated and nonprotonated forms of the nitroxide.

It is clearly seen that that isotropic nitrogen hyperfine splitting constant A_{iso} decreases as pH decreases. A_{iso} at intermediate pH were calculated as weighted averages of the isotropic nitrogen hyperfine couplig constants of the protonated and non-protonated forms of the nitroxide and plotted as a function of pH. The corresponding pK_a values

were obtained (Table 2.2) by fitting the experimental data into the modified Henderson-Hasselbalch equation:

$$A_{iso} = \frac{A_N \times 10^{(pH-pK)} + A_{NH^+}}{1+10^{(pH-pK)}} \quad (2.8)$$

where A_N is the isotropic nitrogen hyperfine splitting constant of EPR spectrum of nonprotonated form of the spin-labeled ligand, and A_{NH+} is the hyperfine splitting constant of EPR spectrum of completely protonated form. Experimental EPR titration curves for the spin-labeled ligand 17 are shown in Fig. 2.30. A linear regression of the experimental pK_a to 100% water is shown in Fig. 2.31. Thus, the intrinsic pK_a of **17** was determined to be pK_a = 3.28±0.33. It should be noted that the titration curves in Fig 2.30 are shifted with respect to each other not only along the X-axis (difference in the pK_a values), but also along the Y-axis (difference in the A_{iso}). The latter effect is explained by the explicit dependence of A_{iso} on the polarity of the environment.

Table 2.2 Titration Data for 12-(acetylthio)dodecyl 3-(3-oxyl-1,2,4,4,5-pentamethylimidazolidin-2-yl)propanoate 17 in Buffer/Isopropanol Solutions of Various Compositions

Vol % isopropanol	$A_{iso}R^{\cdot}$, G	$A_{iso}R^{\cdot}H^{+}$, G	Observed pKa
60	15.0334 ± 0.0030	14.0669 ± 0.0025	1.9333 ± 0.0846
40	15.1268 ± 0.0011	14.1190 ± 0.0012	2.1431 ± 0.0845
20	15.4650 ± 0.0020	14.2307 ± 0.0011	2.8888 ± 0.0643
0	Intrinsic pKa $= 3.28 \pm 0.33$		

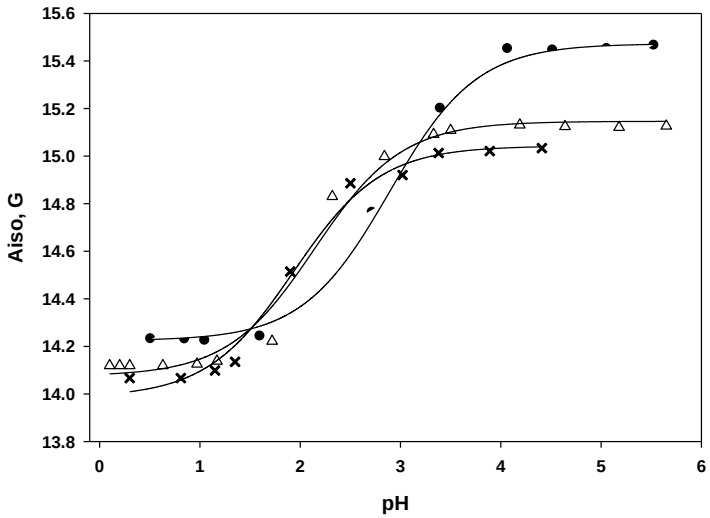

Fig. 2.30 Experimental X-band EPR titration data for 12-(acetylthio)dodecyl 3-(3-oxyl-1,2,4,4,5-pentamethylimidazolidin-2-yl)propanoate (17) measured at room temperature in buffer/isopropanol solutions of the following ratios (v/v): (●) 80:20, (▲) 60:40, (x) 40:60.

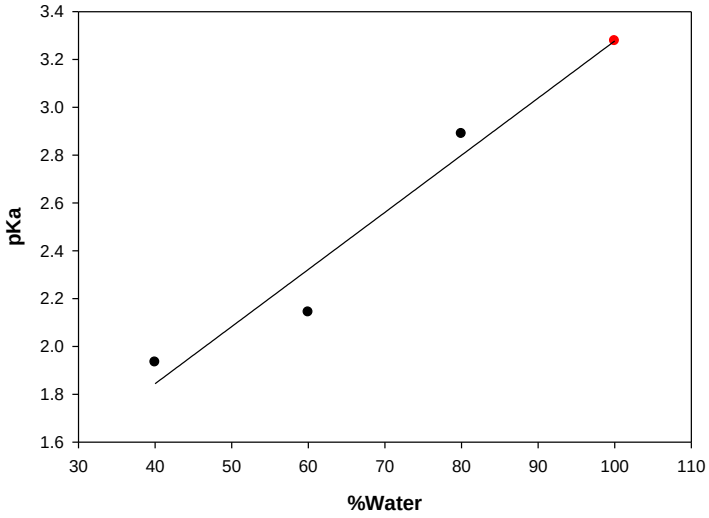

Fig. 2.31 Linear regression of pK_a of 12-(acetylthio)dodecyl 3-(3-oxyl-1,2,4,4,5-pentamethylimidazolidin-2-yl)propanoate (17) vs. percentage of bulk water. pK_a value in bulk water (100% water) was estimated based on this regression.

2.5.2 S-10-oxo-10-(2-(1-oxyl-2,2,5,5-tetramethyl-2,5-dihydro-1H-imidazol-4-ylamino)ethylamino)decyl ethanethioate (**18**)

The intrinsic pK_a of the nitroxide-modified ligand **18** was determined in a similar way. A series of representative X-band EPR spectra of **18** taken in buffer solution-isopropanol mixtures at various pH is shown in Fig. 2.32. Experimental X-band EPR titration data with the least-squares Henderson-Hasselbalch titration curves are shown in Fig. 2.33. A linear regression of the experimental pK_a to 100% water is shown in Fig. 2.34. The intrinsic pK_a of **18** in 100% water was determined to be pK_a = 5.99±0.33. The results of the EPR titration are summarized in Table 2.3.

Table 2.3 Titration Data for S-10-oxo-10-(2-(1-oxyl-2,2,5,5-tetramethyl-2,5-dihydro-1H-imidazol-4-ylamino)ethylamino)decyl ethanethioate 18 in Buffer/Isopropanol Solutions of Various Compositions

Vol % isopropanol	$A_{iso}R^{\cdot}$, G	$A_{iso}R^{\cdot}H^{+}$, G	Observed pKa
60	15.2273 ± 0.0031	14.5568 ± 0.0037	4.2769 ± 0.0673
40	15.3941 ± 0.0012	14.6702 ± 0.0021	4.6089 ± 0.1024
20	15.6629 ± 0.0011	14.8329 ± 0.0013	5.4779 ± 0.0444
0	Intrinsic pKa = 5.99 ± 0.33		

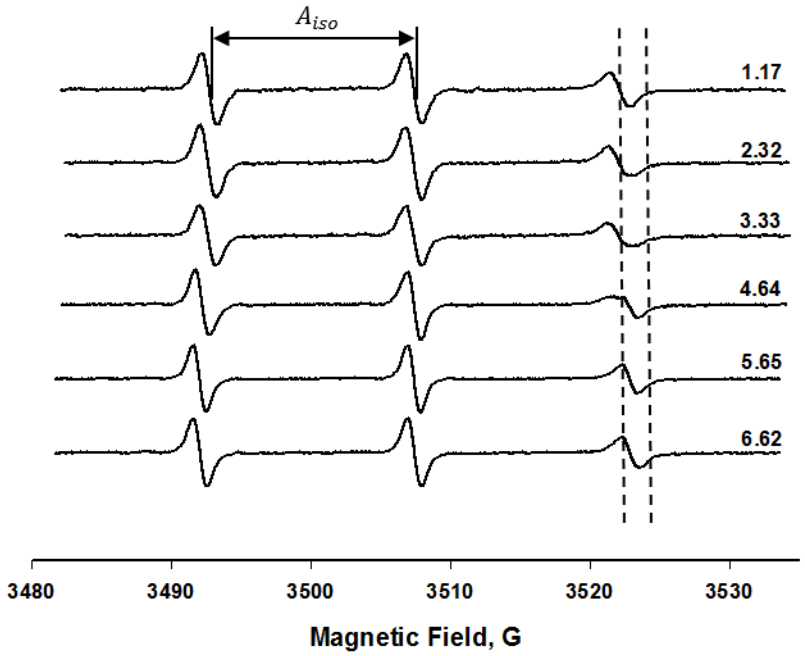

Fig. 2.32 Representative room-temperature X-band EPR spectra of S-10-oxo-10-(2-(1-oxyl-2,2,5,5-tetramethyl-2,5-dihydro-1H-imidazol-4-ylamino)ethylamino)decyl ethanethioate (18) in a series of 40% isopropanol buffer solutions of different pH indicated next to the spectra. Dashed lines mark approximate positions of the high-field nitrogen hyperfine coupling components corresponding to protonated and nonprotonated forms.

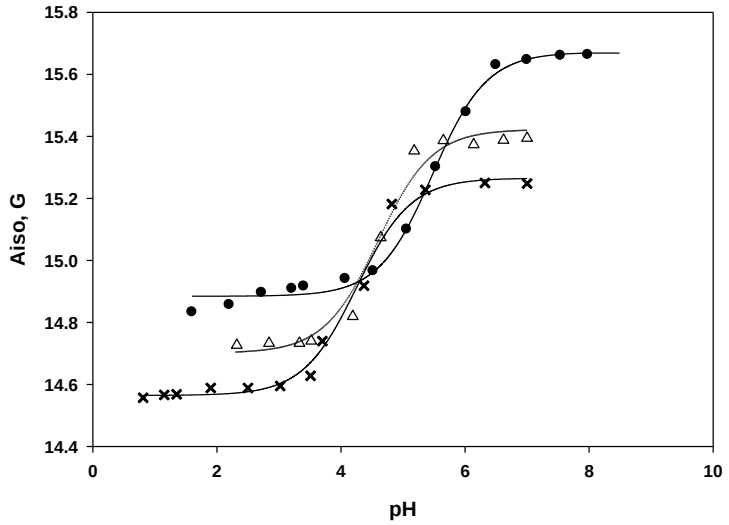

Fig. 2.33 Experimental X-band EPR titration data for S-10-oxo-10-(2-(1-oxyl-2,2,5,5-tetramethyl-2,5-dihydro-1H-imidazol-4-ylamino)ethylamino)decyl ethanethioate (18) measured at room-temperature in buffer/isopropanol solutions of the following ratios (v/v): (●) 80:20, (▲) 60:40, (x) 40:60.

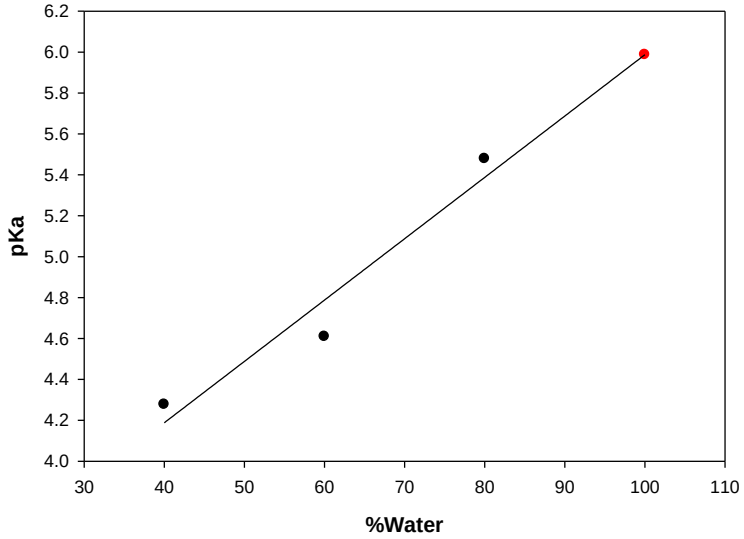

Fig. 2.34 Linear regression of pK_a of S-10-oxo-10-(2-(1-oxyl-2,2,5,5-tetramethyl-2,5-dihydro-1H-imidazol-4-ylamino)ethylamino)decyl ethanethioate (18) vs. percentage of bulk water. pK_a value in bulk water was predicted based on this regression.

2.6 Titration of S-10-oxo-10-(2-(1-oxyl-2,2,5,5-tetramethyl-2,5-dihydro-1H-imidazol-4-ylamino)ethylamino)decyl ethanethioate-modified Au NPs (23)

The intrinsic pK_a of the nitroxide-modified ligand **18** was determined earlier in this project and was found to be pK_a = 5.99±0.33. When attached to the surface of Au NPs, the pK_a of the reporter nitroxide placed at the nanoparticle/bulk water interface is expected to shift to the acidic region of pH due to the destabilization of the protonated form of the nitroxide by a positive charge of coating Thus, to avoid a necessity to carry out our EPR experiments at very acidic pH (to shift them to more "physiological" pH range) we decided to compensate a positive charge of nanoparticles with a negative charge of water-soluble detergent sodium dodecyl sulfate (SDS). Also, using charge compensation has a relevance to biological application of NPs, because an interaction of NPs with such negatively charged polyelectrolytes as nucleic acids would result in a similar effect. Thus, SDS is mimicking the electrostatic properties of nucleic acids, providing a model environment for biological/biophysical applications of spin-labeled Au NPs. There is also another reason why we chose SDS as a dopant for positively charged Au NPs. In our earlier titration and zeta-potential measurement experiments we have found that once the nanoparticle charge is (even partially) neutralized (for example, by adjusting the pH from 3.5 to 7.5 units), the nanoparticles aggregate. A similar effect has also been reported in the literature by others. [28] Thus, we assumed that an SDS shell surrounding the nanoparticles will also prevent them from aggregation when the pH changes (charge is neutralized), which would allow us to experiment with NPs in a much broader pH range.

Experimental X-band (9.5 GHz) EPR spectra of **23** taken at various pH in the presence of SDS (SDS/**5**=4:1) are shown in Fig. 2.35. Using EPR spectra acquired at pH=9.21 (non-protonated form) and pH=1.90 (protonated form) as the reference spectra the experimental EPR spectra acquired at intermediate pH were least-squares decomposed for the individual components corresponding to the non-protonated and protonated forms of the nitroxide using software EWTWO. [27] [29]The normalized intensities obtained by double integration of the spectrum corresponding to each form

allowed us to calculate the fraction of the nonprotonated component for each experimental spectrum (eq. 2.9).

$$f = \frac{I_{(R^{\bullet})}}{I_{(R^{\bullet})} + I_{(R^{\bullet}H^{+})}} \tag{2.9}$$

$I_{(R\bullet)}$ is the normalized intensity of the nonprotonated form of the nitroxide, $I_{(R\bullet H+)}$ is the normalized intensity of the protonated for of the nitroxide.

The fractions were plotted as a function of pH and after the fitting the experimental data into the Henderson-Hasselbalch equation (Fig. 2.36), the corresponding pK_a value was found to be 7.27±0.04.

Fig. 2.35 (a) Representative room-temperature X-band EPR spectra of S-10-oxo-10-(2-(1-oxyl-2,2,5,5-tetramethyl-2,5-dihydro-1H-imidazol-4-ylamino)ethylamino)decyl ethanethioate-modified Au NPs (23) taken at various pH in a series of aqueous solutions in the presence of SDS (SDS/5=4:1). pH of the solutions are indicated next to the corresponding spectra. (b) EPR spectra comparison of 23-modified Au NPs in completely protonated and free forms.

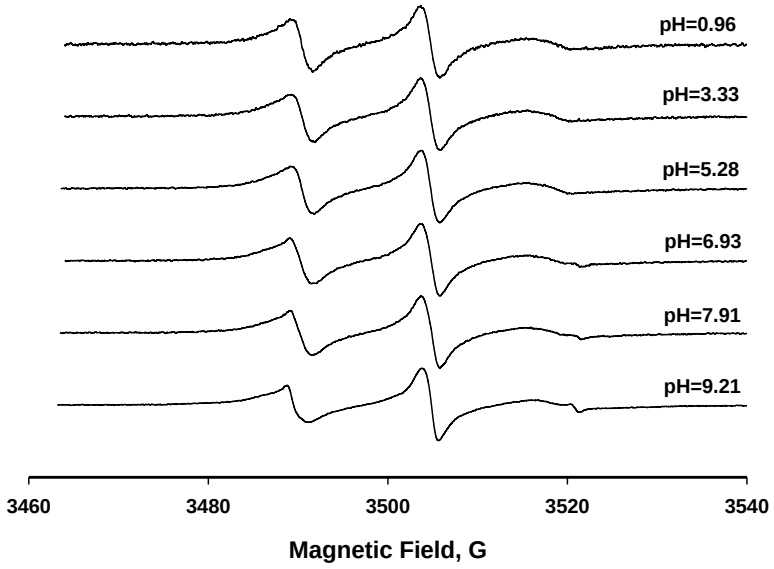
pH=0.96
pH=3.33
pH=5.28
pH=6.93
pH=7.91
pH=9.21
3460
3480
3500
3520
3540
Magnetic Field, G

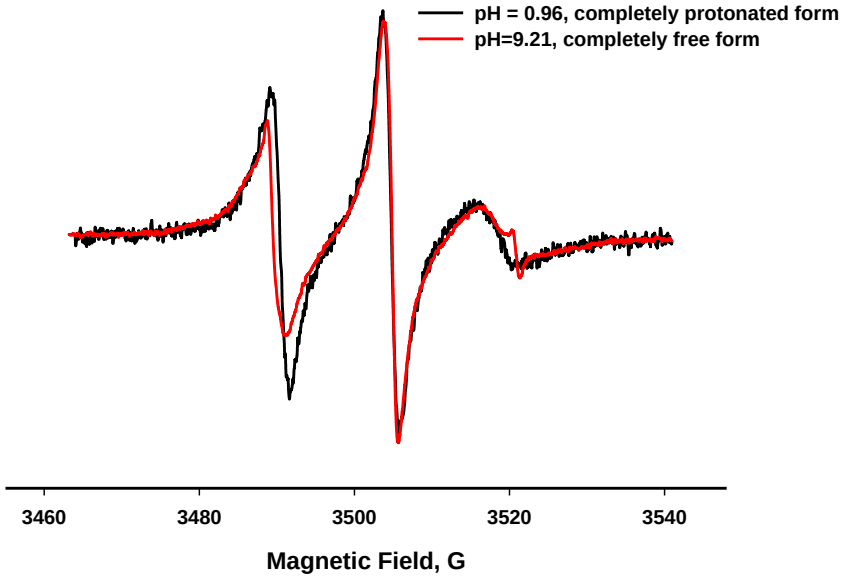
pH = 0.96, completely protonated form
pH=9.21, completely free form
3460
3480
3500
3520
3540
Magnetic Field, G

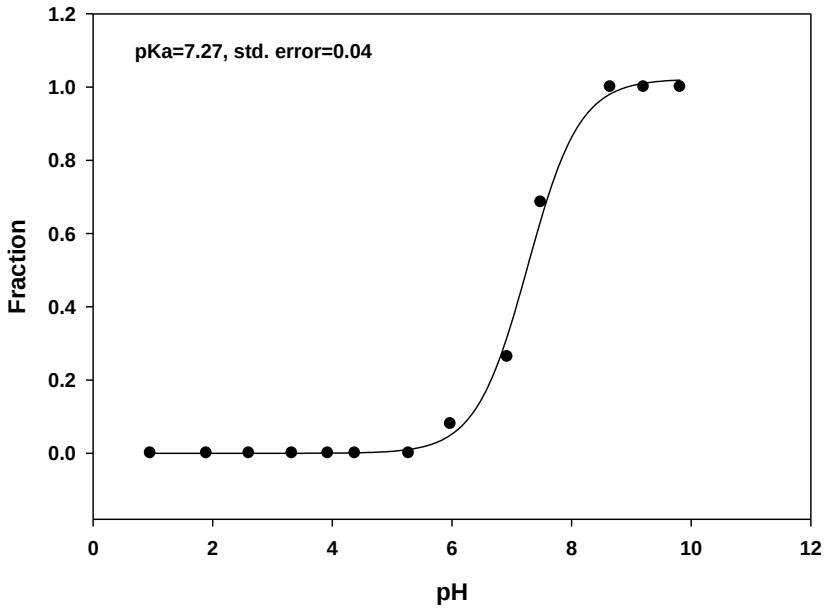

Fig. 2.36 EPR titration data for S-10-oxo-10-(2-(1-oxyl-2,2,5,5-tetramethyl-2,5-dihydro-1H-imidazol-4-ylamino)ethylamino)decyl ethanethioate-modified Au NPs (23). A corresponding Henderson-Hasselbalch titration curve is shown as a solid line.

2.7 Conclusions

1. A new series of disulfide and thioacetate ligands **15-18** modified both with the pH-sensitive and non-pH-sensitive nitroxides has been synthesized through DCC/DMAP-mediated coupling reactions for spin-labeling of the ligand-protected gold nanoparticles.

2. Intrinsic pK_a's of the hydrophobic and insoluble in water ligands **17** and **18** modified with the pH-sensitive nitroxide were determined by EPR pH titration of these ligands in a series of buffer solution-isopropanol mixtures varying the concentration of the isopropanol. The pK_a's experimentally obtained in these mixtures were extrapolated to 100% water.

3. The nitroxide-modified disulfide ligand was found not to be effective in the ligand-exchange reaction with Au NPs decorated with long (C_9-C_{12}) ligands. The nitroxide-

modified thioacetate ligands were found to be much more suitable for spin-labeling of the Au NPs coated with long ligands through the ligand exchange reaction. A series of spin-labeled Au nanoparticles was synthesized through the ligand exchange reaction with the nitroxide-modified thioacetate ligands.

4. We have found that the use of sodium dodecyl sulfate as a dopant for positively charged Au NPs in solution prevents the NPs aggregation when the nanoparticles' charge is neutralized.

5. Interfacial pK_a of the pH-sensitive nitroxide ligand **18** embedded into the positively charged coating monolayer of Au NPs was determined through EPR pH titration.

6. Overall, an advanced spin probe EPR-based approach for studying the ligand shell dynamics, interfacial electrostatic interactions, and interfacial proton transfer-related phenomena in the ligand-protected gold nanoparticles has been developed.

CHAPTER 3 EXPERIMENTAL PART

3.1 Instruments and Materials

DLS measurements were carried out using a Malvern (Malvern Instruments Inc., Westborough, MA) Zetasizer.

EPR measurements were carried out with a Bruker (Bruker Biospin Inc., Billerica, MA) ELEXSYS E500 spectrometer at approximately 9.5 GHz (X-band) at room temperature.

pH measurements were carried out using a VWR(Radnor, PA) Symphony pH meter sb70p.

Diphenyl Ether, THF, was purchased from Alfa Aesar.

Sodium chloride, Hexanes, Potassium Chloride, Sodium hydroxide, DMSO, Dichloromethane, Potassium Thioacetate (98%), Hydrogen Tetrachloroaurate, Manganese Dioxide (99%), Sodium Borohydride were purchased from Fisher Sci.

Chloroform, Ether, Methyl Alcohol (Anhydrous) were purchased from VWR.

Methanol-D4 was purchased from Cambridge Isotope Laboratories.

Acetic acid, Ammonium acetate, Magnesium Sulfate (Anhydrous), Sodium Sulfate (Anhydrous), Sodium Dodecyl Sulfate were purchased from EMD.

Ethyl acetate, Acetonitrile were purchased from Burdick & Jackson CC.

Iodine, (99.5%) was purchased from Lancaster.

12-Bromo-1-dodecanol (98%), 10-Bromodecanoic acid, (95%), DCC (99%), 4-(Dimethylamino)pyridine (99%), 11-Bromo-1-undecene (95%), Thioacetic Acid (96%), Azobisisobutyronitrile (12 wt. % in acetone), 1-Octanethiol (98.5%), Ethyl Levulinate (98%), Dimethyl sulfate (99%), 11-Mercapto-1-undecanol (97%), Pyridine (Anhydrous, 99.8%), sodium thiosulfate were purchased from Sigma-Aldrich.

TLC plastic sheets were purchased from Merck.

3-Carboxy-2,2,5,5-tetramethyl-3-pyrroline-1-oxyl (**1**), hydroxyamino ketone (**10**), 4-(2-Aminoethylamino)-1-oxyl-2,2,5,5-tetramethyl-2,5-dihydro-1H-imidazole (**3**) were provided by Dr. Maxim A. Voinov, and all of them are commercially available.

3.2 Synthesis of Ligands

3.2.1 Synthesis of 11-(dimethylamino)undecane-1-thiol hydrochloride (**5**)

This ligand was synthesized as described in references. [6]

1. Synthesis of thioacetic acid-S-(11-bromoundecyl) ester. [6a]

   This reaction is shown in Fig. 3.1.

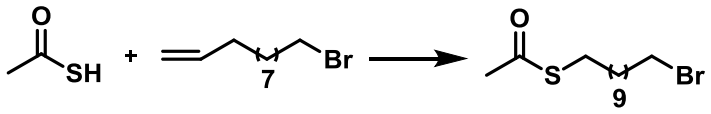

Fig. 3.1 Scheme of synthesis of thioacetic acid-S-(11-bromoundecyl) ester.

11-bromo-1-undecene (10.0 g, 42.9 mmol), thioacetic acid (15.5 ml, 214.5 mmol), and AIBN (3.52 g, 21.45mmol) were dissolved in dry toluene (250ml). The solution was thoroughly flushed with Argon gas and the reaction was carried out under Argon atmosphere. The reaction mixture was refluxed upon vigorous stirring for 4 hrs. The resulting mixture was cooled down to room temperature and diluted with diethyl ether (1L). The organic layer was separated and washed with DI water (3×500mL) and with brine (1×500mL). The organic layer was dried over Na_2SO_4 overnight, and solvents were evaporated under reduced pressure. The crude product was purified by chromatography on silica gel using hexane/CH_2Cl_2 mixture (2:1) as an eluent. Pure thioacetic acid-S-(11-bromoundecyl) ester was obtained as slightly yellow oil (12.90 g,

97.3%). ^{1}H NMR (400 MHz, $CDCl_3$, δ): 3.41(t, 2H, CH_2Br), 2.86(t, 2H, CH_2S), 2.32(s, 3H, CH_3CO), 1.85 (q of t, 2H, $BrCH_2CH_2$), 1.56(m, 2H, SCH_2CH_2), 1.28(m, 14H). The NMR spectrum is shown in Fig. 3.2.

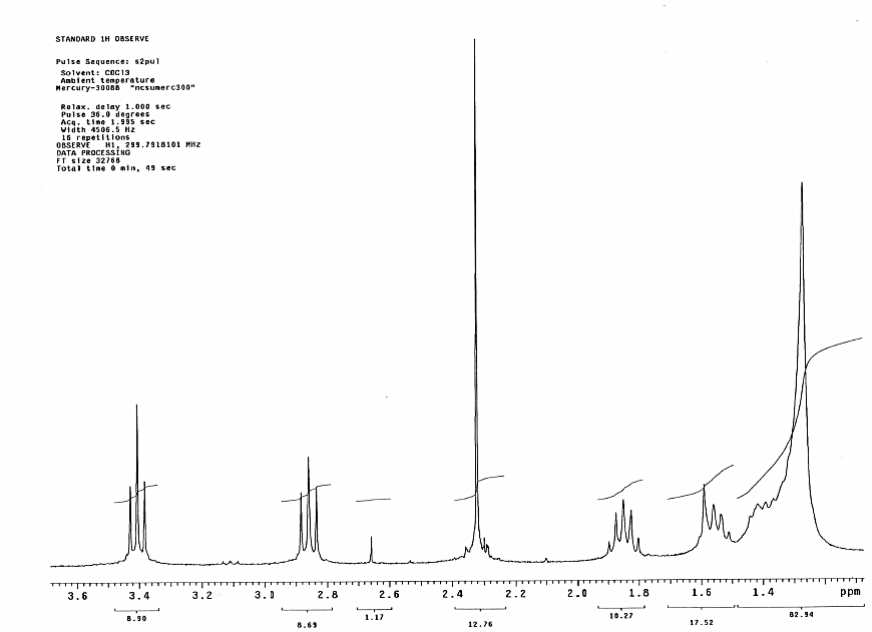

Fig. 3.2 The ^{1}H NMR spectrum of thioacetic acid-S-(11-bromoundecyl) ester.

2. Synthesis of **5**. [6b]

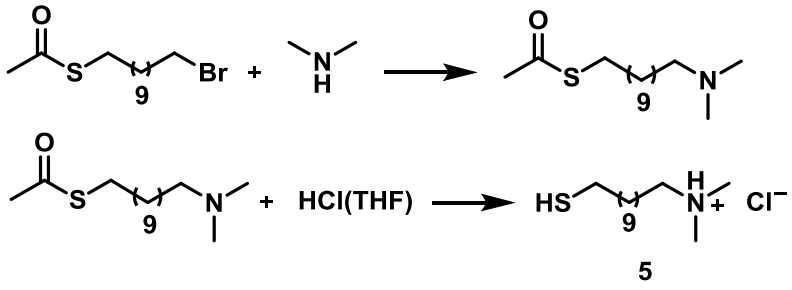

Fig. 3.3 Scheme of the synthesis of 11-(dimethylamino)undecane-1-thiol hydrochloride (5).

Dimethylamine (376 mmol, 4.78 ml) was dissolved in THF (188 ml), and cooled to 0^{o}C. A solution of thioacetic acid-S-(11-bromoundecyl) ester (8.5617 g, 28.8mmol) in 40 ml of THF was slowly added to the dimethylamine solution over a period of 6 hrs; the reaction was vigorously stirred during this period. The reaction was stirred for another 36 hrs at room temperature, then the solvent was evaporated under reduced pressure. The resulting crude product was purified by chromatography on silica gel using CH_2Cl_2/MeOH/AcOH mixture (89:10:1) as an eluent. The fraction containing pure 11-(dimethylamino)undecane-1-thiol was concentrated under reduced pressure. Purified 11-(dimethylamino)undecane-1-thiol was converted into the corresponding hydrochloride. For this purpose dimethylamino derivative was taken up in 20% solution of gaseous HCl in THF. Solvent was removed under reduced pressure and treatment with HCl/THF was repeated again. To assure the complete conversion of the dimethylamino derivative to the corresponding hydrochloride, this procedure was repeated several times. Finally, the solvent was removed under reduced pressure yielding **5** as a white powder (2.5000 g, 32.6%). ^{1}H NMR (400 MHz, CD_3OD, δ): 3.23(s, 2H, HS+NH), 3.05(m, 2H, $CH_2NH(Me)_2$), 2.79(s, 6H, $NH(Me)_2$), 2.40(t, 2H, $HSCH_2$), 1.64(m, 2H, CH_2CH_2NH), 1.50(q, 2H, $HSCH_2CH_2$), 1.20-1.38(m, 14H). The NMR spectrum is shown in Fig. 3.4.

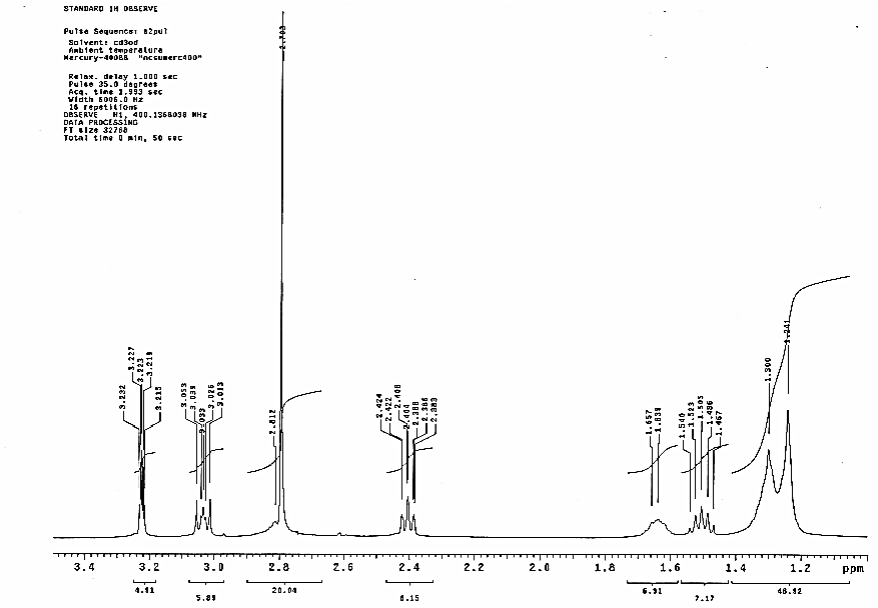

Fig. 3.4 ^{1}H NMR spectrum of 11-(dimethylamino)undecane-1-thiol hydrochloride (5).

The IR spectrum of **5** is shown in Fig. 3.5. The absorption peaks at 2921, 2851cm^{-1} can be assigned to CH stretching vibrations and peaks at 1472, 730 cm^{-1} can be assigned to CH_2 bending vibrations. Peak at 2676 cm^{-1} is assigned to the scissoring vibrations of $(CH_3)_3NH^+$ group.

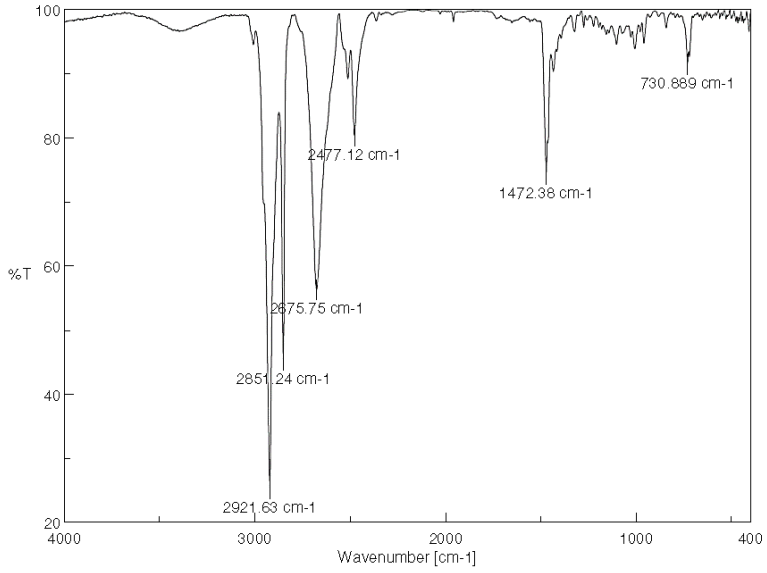

Fig. 3.5. IR spectrum of 11-(dimethylamino)undecane-1-thiol hydrochloride (5).

3.2.2 Synthesis of 11, 11'-Dithiodiundecanol (**7**).

7 was synthesized through oxidative coupling of **6** using literature procedures. [13-14]

In these syntheses, iodine and DMSO were used as oxidants.

Method 1[14]:

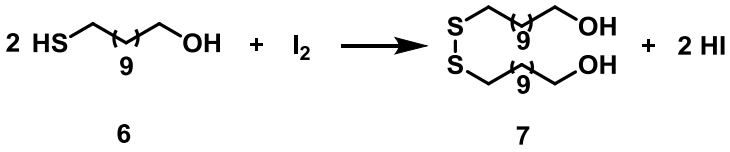

6 **7**

Fig. 3.6 Scheme of the synthesis of 11, 11'-Dithiodiundecanol (7).

6 (500 mmg, 2.45 mmol) was dissolved in 12 ml of H_2O/CH_3CN mixture (1:5). Pyridine (197.5 µL, 2.45 mmol) and iodine (311.15 mg, 1.23 mmol) were consecutively added to the solution upon vigorous stirring. The completion of the reaction was monitored

by TLC. After completion of the reaction, the mixture was washed with 10 mL of 1% $Na_2S_2O_3$ solution to remove the excess of iodine. 11,11'-Dithiodiundecanol was extracted with CH_2Cl_2 and dried over Na_2SO_4 overnight. CH_2Cl_2 was evaporated under reduced pressure and the solidified 11,11'-dithiodiundecanol was recrystallized from the mixture of CH_3CN and CH_3OH. 11,11'-Dithiodiundecanol was obtained as a white powder. (521.9 mg, 52.3%). Melting point (MP) =79 ^{0}C.

Method 2:

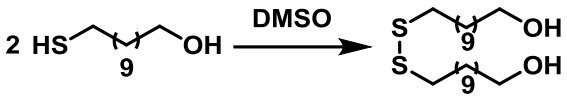

Fig. 3.7 Scheme of the synthesis of 11, 11'-Dithiodiundecanol (7).

DMSO (87 µL, 1.23 mmol) was added to a solution of **6** (100 mmg, 0.49 mmol) in 2 ml of H_2O:CH_3CN mixture (1:5), the resulting solution was thoroughly flushed with Argon and heated at 120 ^{0}C upon stirring for 16 hrs. After the reaction mixture cooled down, it was extracted with CH_2Cl_2 and the organic extract was dried over Na_2SO_4 overnight. CH_2Cl_2 was evaporated under reduced pressure and the solid 11,11'-dithiodiundecanol was recrystallized from the mixture of CH_3CN and CH_3OH. Yield: 38.5 mg, 38.7%.

Structure of **7** we have synthesized was verified by ^{1}H NMR (400 MHz, $CDCl_3$, δ): 3.62 (t, 4H, CH_2OH), 2.66 (t, 4H, SCH_2), 1.65 (q, 4H, SCH_2CH_2), 1.55 (m, 6H, CH_2CH_2OH), 1.32 (m, 28H, CH_2), (Fig. 3.8).

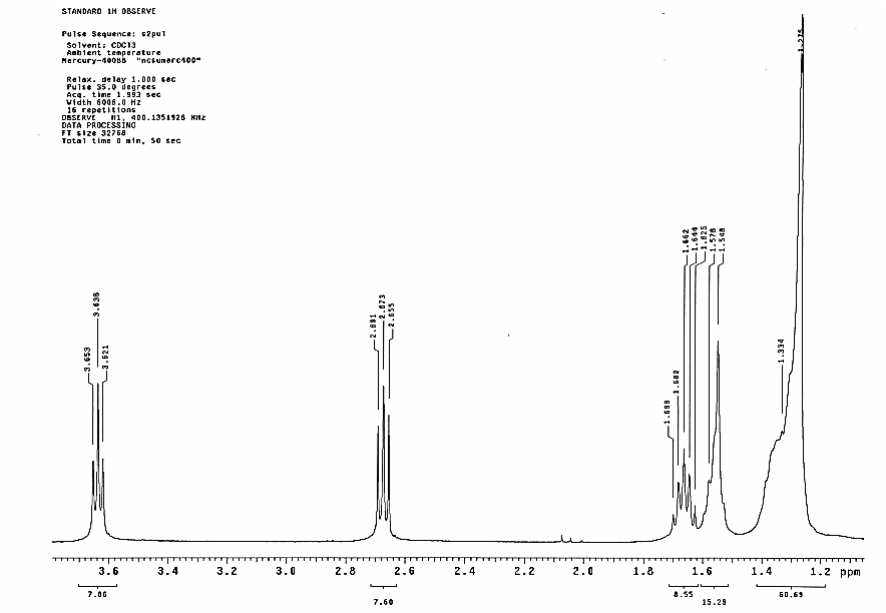

Fig. 3.8 ^{1}H NMR spectrum of 11, 11'-Dithiodiundecanol (7).

3.2.3 Synthesis of 12-(Acetylthio)dodecanol (**8**).

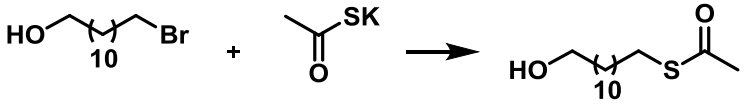

Fig. 3.9 Scheme of the synthesis of 8.

8 was synthesized using literature procedures. [16]

Potassium thioacetate (273.6 mg, 2.4 mmol) was added at 0 ^{o}C to a solution of 12-bromo-1-dodecanol (424.0 mg, 1.6 mmol) in 8 mL of dry DMF and the reaction mixture was stirred at room temperature overnight. The reaction mixture was diluted with DMSO (8 mL) and ethyl acetate (16 mL) and washed with brine (3×25 mL). The organic layer was dried by Na_2SO_4, and the solvent was evaporated under reduced

pressure. The crude solidified product was recrystallized from hexanes, giving **8** as a white crystalline product (266.3 mg, 64%). MP=54-56 ^{0}C. ^{1}H NMR (400 MHz, $CDCl_3$, δ): 3.64 (t, 2H,CH_2OH), 2.86 (t, 2H, CH_2S), 2.33 (s, 3H, CH_3), 1.56 (m, 4H, $HOCH_2CH_2$, CH_2CH_2S), 1.20-1.42 (m, 16H, CH_2), (Fig. 3.10).

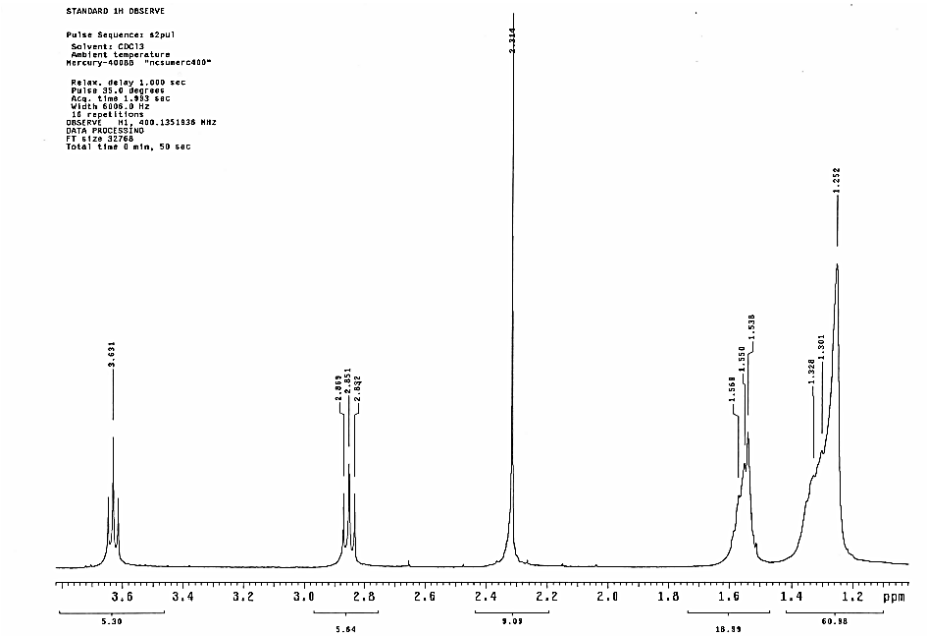

Fig. 3.10 ^{1}H NMR spectrum of 12-(Acetylthio)dodecanol (8).

3.2.4 Synthesis of 10-(Acetylthio)decanoic acid (**9**).

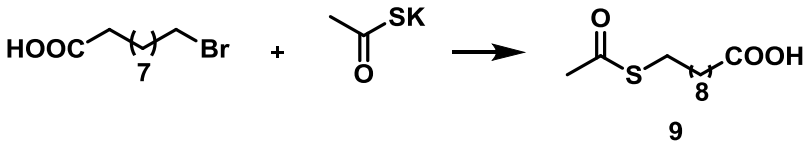

9

Fig. 3.11 Scheme of the synthesis 10-(Acetylthio)decanoic acid (9).

9 was synthesized using literature procedures. [16]

Potassium thioacetate (670.2 mmg, 5.9 mmol) was added at 0 ^{o}C to a solution of 10-bromodecanoic acid (983.7 mg, 3.9 mmol) in 16 ml of dry DMF and the reaction mixture was stirred at room temperature overnight. The reaction mixture was diluted with DMSO (16 mL) and ethyl acetate (32 mL) to wash out DMF and washed with brine (3×50 mL). The organic layer was dried by Na_2SO_4, and the solvent was evaporated under reduced pressure. The crude solid product was recrystallized from hexanes affording **9** as light yellow crystals (481 mg, 50.1%). ^{1}H NMR (300 MHz, $CDCl_3$, δ ,): 2.85 (t, 2H, CH_2S), 2.34 (m, 5H, CH_3+CH_2COOH), 1.59 (m, 4H, CH_2CH_2COOH+CH_2CH_2S), 1.24-1.40 (m, 10H, CH_2), (Fig. 3.12).

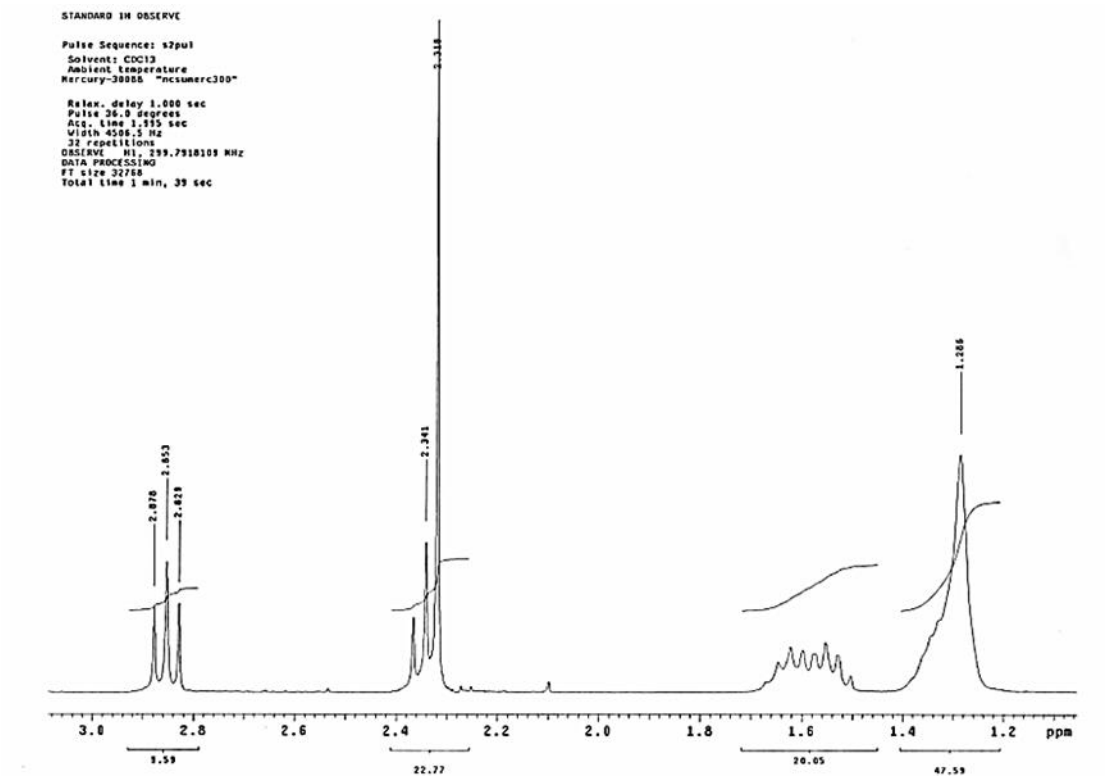

Fig. 3.12 ^{1}H NMR spectrum of 10-(Acetylthio)decanoic acid (9).

3.3 Synthesis of Nitroxide Radicals

The synthesis of nitroxide radical 2 is based on methods from literature. [18]

3.3.1 Synthesis of 1-hydroxy-3-imidazoline derivative (**11**).

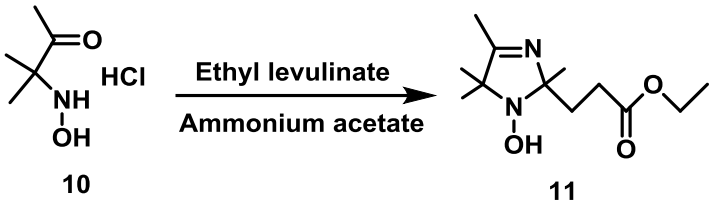

Fig. 3.13 Scheme of the synthesis of 1-hydroxy-3-imidazoline derivative (11).

10 (3.00 g, 19.4 mmol), ethyl levulinate (3.17 g, 22.0 mmol) and ammonium acetate (6.17 g, 80.1 mmol) were dissolved in methanol (50 mL), the flack was placed into an oil bath and the reaction mixture was refluxed for 3-5 hrs. Completion of reaction was monitored by TLC. The reaction mixture was allowed to cool, solvents were removed under reduced pressure, the precipitate formed was collected on a filter and washed with ultra-pure water. **11** was obtained as light yellow crystals (3.2g, 68%). MP=141-145^{0}C.

3.3.2 Synthesis of corresponding radical of 1-hydroxy-3-imidazoline derivative (**12**).

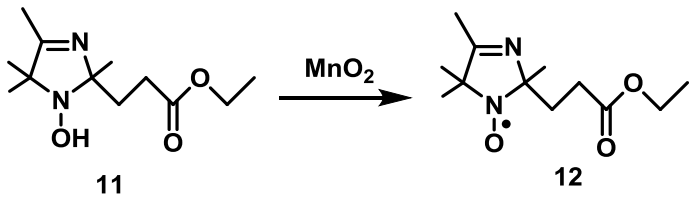

Fig. 3.14 Scheme of the synthesis of corresponding radical of 1-hydroxy-3-imidazoline derivative (12).

11 (6.26 g, 25.9 mmol) was dissolved in chloroform (50 mL), and manganese dioxide (4.3 g, 49.5 mmol) was added. The reaction mixture was stirred at room temperature for 4 hrs. Excess of the oxidant was filtered off, solvent was removed under reduced pressure, giving chromatographically pure **12** (6.24 g, 100%). The product was used without further purification.

3.3.3 Synthesis of 2-(2-methoxycarbonylethyl)-2,3,4,5,5-pentamethyl-3-imidazolinium 1-oxyl methylsulfate (**13**).

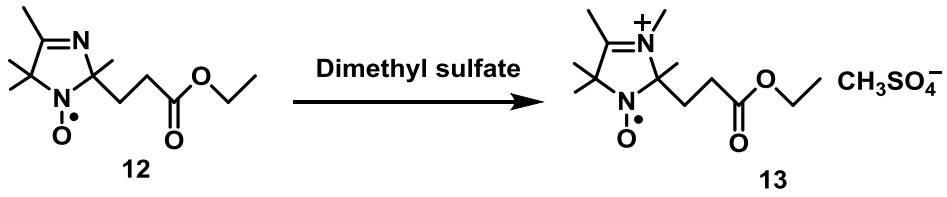

Fig. 3.15 Scheme of the synthesis of 2-(2-methoxycarbonylethyl)-2,3,4,5,5-pentamethyl-3-imidazolinium 1-oxyl methylsulfate (13).

Dimethyl sulfate (5.67 mL, 59.9 mmol) was added to a solution **12** (6.24 g, 25.9 mmol) in dry ether (45 mL), and the reaction mixture was allowed to stay at room temperature for 20 min. Ether was slowly evaporated under slightly reduced pressure using a rotary evaporator. After complete evaporation of ether, the flask with the reaction mixture was kept on a rotary evaporator under reduced pressure for 40 min. During this time the reaction mixture solidified. The solid residue was triturated with ether; the precipitate was collected on a filter and washed with ether. The precipitate was re-crystallized from a mixture of ethyl acetate and methanol, affording **13** as a light yellow powder (4.74 g, 49.9%).

3.3.4 Synthesis of 2-(2-methoxycarbonylethyl)-2,3,4,5,5-pentamethylimidazolidine 1-oxyl (**14**).

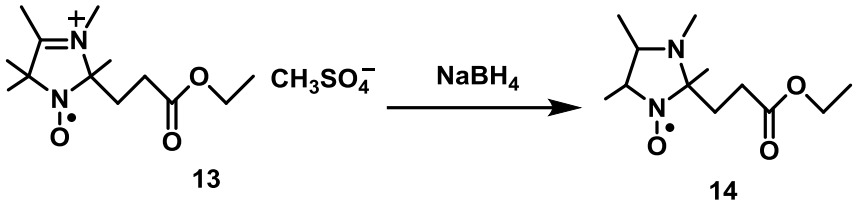

Fig. 3.16 Scheme of the synthesis of 2-(2-methoxycarbonylethyl)-2,3,4,5,5-pentamethylimidazolidine 1-oxyl (14).

Sodium borohydride (51.03 mg, 1.35 mmol) was dissolved in ice-cold water (1.3 mL), a solution was kept at 0 ^{o}C for 30 min and then added upon stirring to a solution of **13** (329.3 mg, 0.9 mmol) in the two-phase mixture of ultra-pure water (1.30 mL) and dichloromethane (2.53 mL) cooled to 0 ^{o}C. The reaction mixture was stirred at room temperature for 10 min, then organic layer was separated and dried over $MgSO_4$ overnight. Solvent was evaporated under reduced pressure. **14** forms as a mixture of diastereomers which were separated by chromatography on silica gel using a mixture of hexane/ethyl acetate (2:1) as an eluent (diastereomer A: 95.6 mg, 41.3%, diastereomer B: 45.5 mg, 19.7%).

The IR spectra of the diastereomers are very similar to each other (Fig. 3.17). Both IR spectra show a strong absorption band around 1730 cm^{-1} (1733 cm^{-1} for diastereomer A and 1735 cm^{-1} for diastereomer B) characteristic to the valence vibration of C=O bond in the ester group.

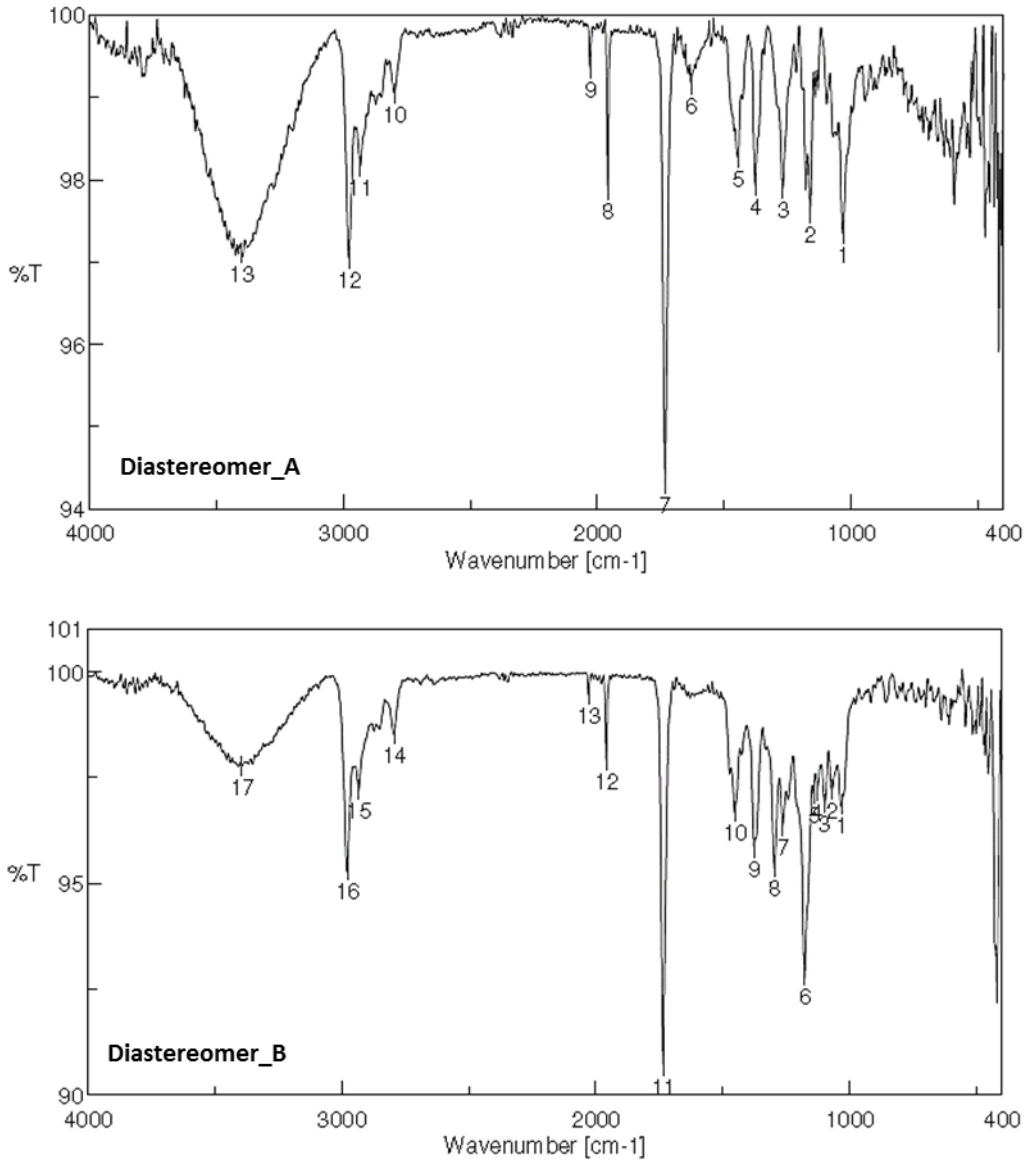

Fig. 3.17 IR spectra of the diastereomers of 2-(2-methoxycarbonylethyl)-2,3,4,5,5-pentamethylimidazolidine 1-oxyl (14).

Structures of the diastereomers synthesized were also verified by mass-spectroscopy. Mass spectrum: calcd for $C_{13}H_{25}N_2O_3$ 257.19 (M^+), found 258.19 $(M+H)^+$ (Fig. 3.18).

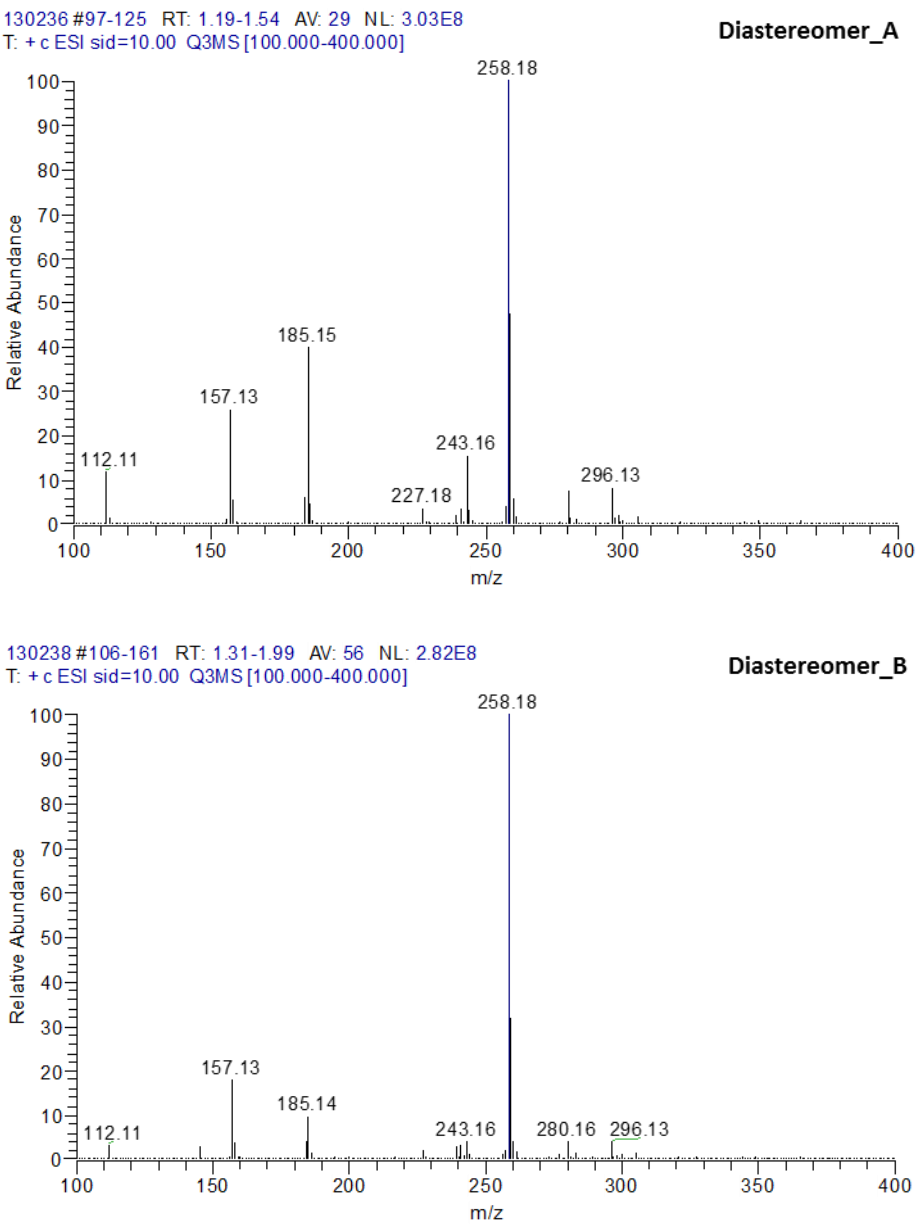

Fig. 3.18 Mass spectra of the diastereomers of 2-(2-methoxycarbonylethyl)-2,3,4,5,5-pentamethylimidazolidine 1-oxyl (14).

3.3.5 Synthesis of 2-(2-Carboxyethyl)-2,3,4,5,5-pentamethylimidazolidine-1-oxyl (**2**).

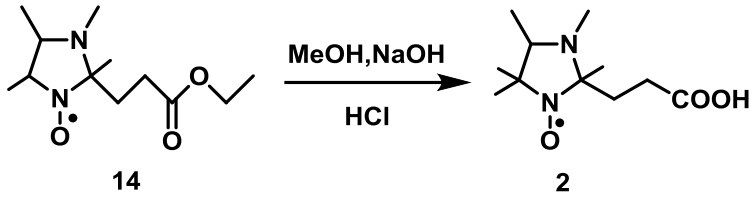

Fig. 3.19 Scheme of the synthesis of 2-(2-Carboxyethyl)-2,3,4,5,5-pentamethylimidazolidine-1-oxyl (2).

Diastereomer A (the one with a higher R_f value) of the **14** (95.6 mg, 0.37 mmol) was dissolved in a mixture of ultra-pure water and methanol (water/methanol=1/100) and 3 M NaOH solution was added drop by drop until **14** vanished on TLC on silica gel (eluent: hexane/ethyl acetate, 2:1). As follows from the TLC analysis, during the course of the reaction the diastereomer A first slowly converted to the diastereomer B (confirmed by IR spectroscopy) and then, after the additional amount of NaOH solution was added, hydrolyzed to the corresponding carboxylic acid derivative. After completion of the reaction, 0.5 M HCl solution was added drop by drop to adjust the pH of the reaction mixture to pH=5-6, and the nitroxide carboxylic acid was extracted with chloroform. Organic extract was dried over Na_2SO_4, the solvent was evaporated under reduced pressure affording **2** as a yellow crystalline product (42.4 mg, 50.0%). IR spectrum of **2** is given in Fig. 3.20.

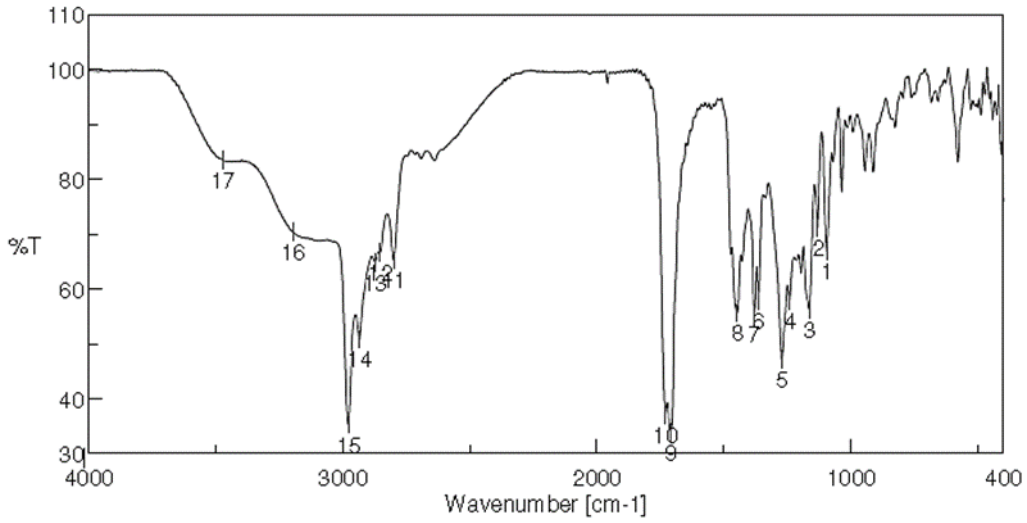

Fig. 3.20 IR spectrum of 2-(2-Carboxyethyl)-2,3,4,5,5-pentamethylimidazolidine-1-oxyl (2).

3.4 Synthesis of Spin-labeled Ligands

Spin labeled ligands were synthesized based on DCC-mediated coupling reactions. [15]

3.4.1 Synthesis of 1,2-bis(undecyl 1-oxyl-2,2,5,5-tetramethyl-2,5-dihydro-1H-pyrrole-3-carboxylate) disulfide (**15**)

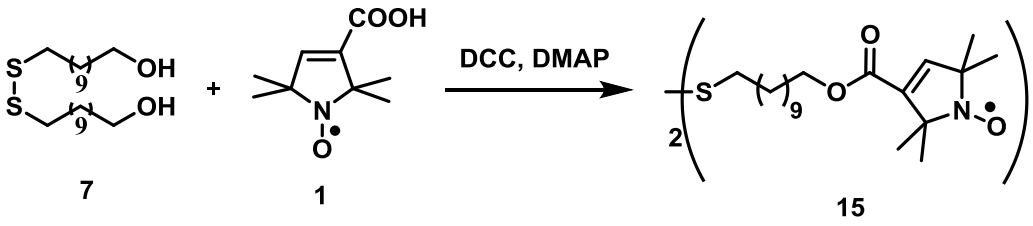

Fig. 3.21 Scheme of the synthesis of 1,2-bis(undecyl 1-oxyl-2,2,5,5-tetramethyl-2,5-dihydro-1H-pyrrole-3-carboxylate) disulfide (15).

7 (50 mg, 1.229×10^{-4}mol), DCC (76.1 mg, 3.687×10^{-4}mol) and DMAP (0.76 mg, 6.145×10^{-6}mol) were dissolved in 2 mL of dry chloroform and a solution of **1** (50.0

mg, 2.704×10^{-4}mol) in 0.5 mL of dry chloroform was added slowly to the mixture. The reaction mixture was stirred at room temperature for 24 hrs, concentrated under reduced pressure and separated by PTLC on silica gel (eluent: methanol/chloroform, 1:300).

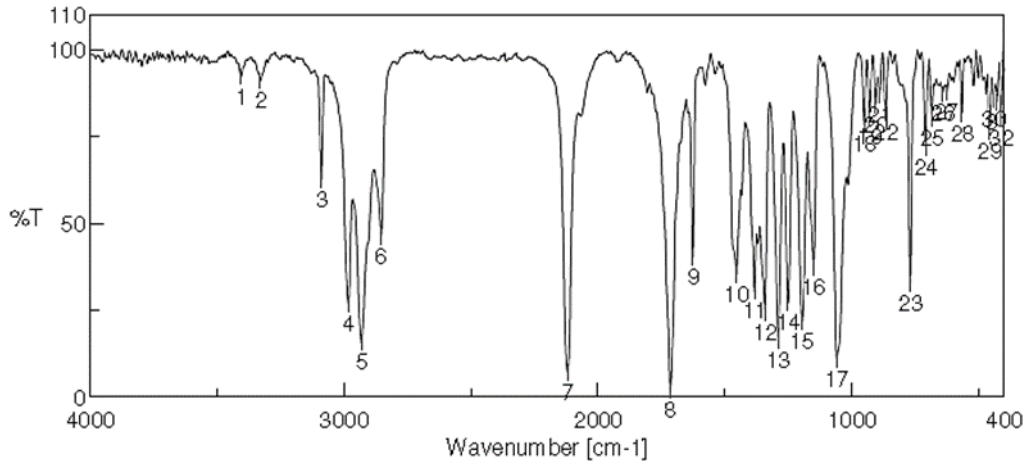

Fig. 3.22 IR spectrum of 1,2-bis(undecyl 1-oxyl-2,2,5,5-tetramethyl-2,5-dihydro-1H-pyrrole-3-carboxylate) disulfide (15). A strong absorption band at 1715 cm $^{-1}$ is characteristic of the stretch vibration of C=O bond in the conjugated ester group. A strong band at 2119 cm $^{-1}$ was attributed to the absorption of an admixture of unreacted DCC (N=C=N group).

3.4.2 Synthesis of 12-(acetylthio)dodecyl 1-oxyl-2,2,5,5-tetramethyl-2,5-dihydro-1H-pyrrole-3-carboxylate (**16**)

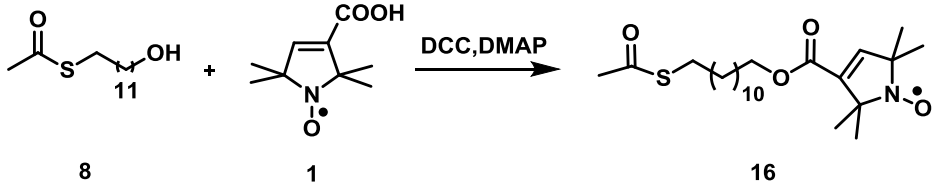

Fig. 3.23 Scheme of the synthesis of 12-(acetylthio)dodecyl 1-oxyl-2,2,5,5-tetramethyl-2,5-dihydro-1H-pyrrole-3-carboxylate (16).

8 (50 mg, 1.923×10^{-4}mol), DCC (59.5 mg, 2.885×10^{-4}mol) and DMAP (0.7 mg) were dissolved in 2 mL of dry chloroform, and a solution of **1** (39.1 mg, 2.1153×10^{-4}mol) in 0.5 mL of dry chloroform was added slowly to the mixture. The reaction mixture was stirred at room temperature for 24 hrs, concentrated under reduced pressure and separated by PTLC on silica gel (eluent: chloroform).

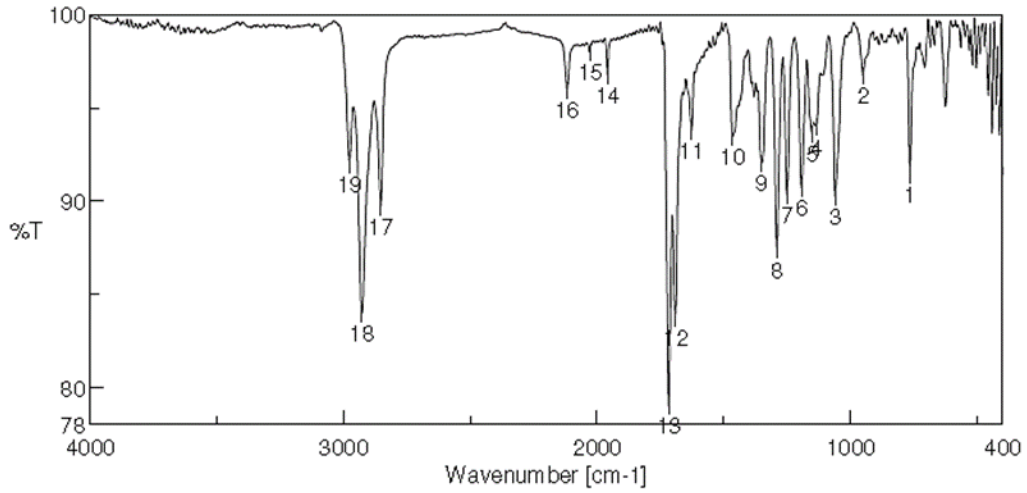

Fig. 3.24 IR spectrum of 12-(acetylthio)dodecyl 1-oxyl-2,2,5,5-tetramethyl-2,5-dihydro-1H-pyrrole-3-carboxylate (16). A strong absorption band at 1717 cm $^{-1}$ is characteristic of the stretch vibration of C=O bond in the conjugated ester group. An absorption band at 1692 cm $^{-1}$ was assigned to the stretch vibration of C=O bond in the thioacetyl group.

3.4.3 Synthesis of 12-(acetylthio)dodecyl 3-(3-oxyl-1,2,4,4,5-pentamethylimidazolidin-2-yl)propanoate (**17**)

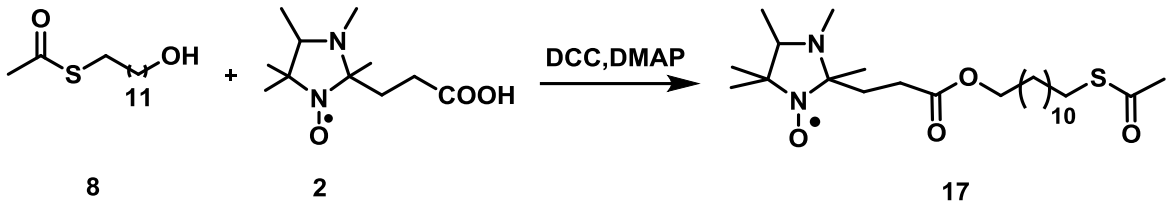

Fig. 3.25 Scheme of the synthesis of 12-(acetylthio)dodecyl 3-(3-oxyl-1,2,4,4,5-pentamethylimidazolidin-2-yl)propanoate (17).

8 (43.7 mg, 1.681×10^{-4}mol), DCC (52.0 mg, 2.520×10^{-4}mol) and DMAP (0.6 mg) were dissolved in 2 mL of dry chloroform and a solution of **2** (42.4 mg, 1.852×10^{-4}mol) in 0.5 mL of dry chloroform was added slowly to the mixture. The reaction mixture was stirred at room temperature for 24 hrs, concentrated under reduced pressure and separated by PTLC on silica gel (eluent: hexane/ethyl acetate, 2:1).

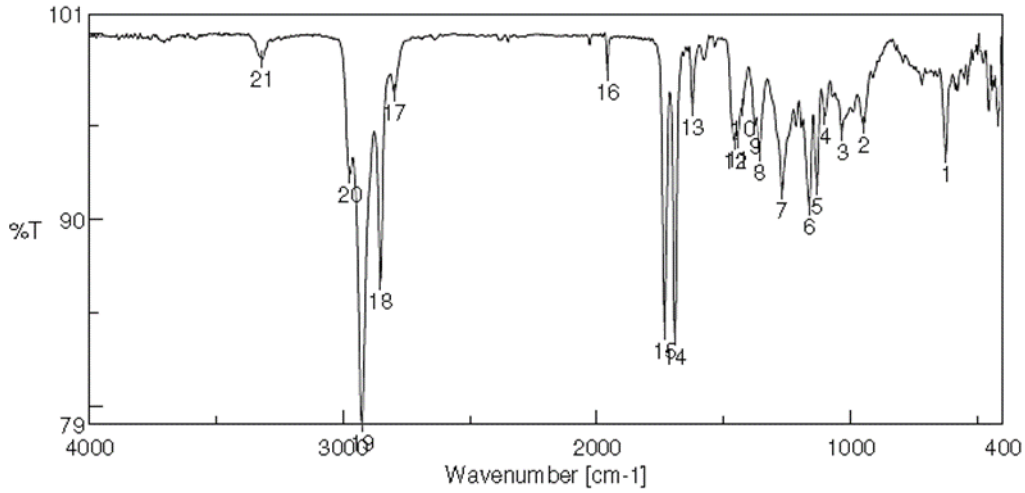

Fig. 3.26 IR spectrum of 12-(acetylthio)dodecyl 3-(3-oxyl-1,2,4,4,5-pentamethylimidazolidin-2-yl)propanoate (17). A strong absorption band at 1733 cm $^{-1}$ is characteristic of the stretch

vibration of C=O bond in the ester group. An absorption band at 1693 cm $^{-1}$ was assigned to the stretch vibration of C=O bond in the thioacetyl group.

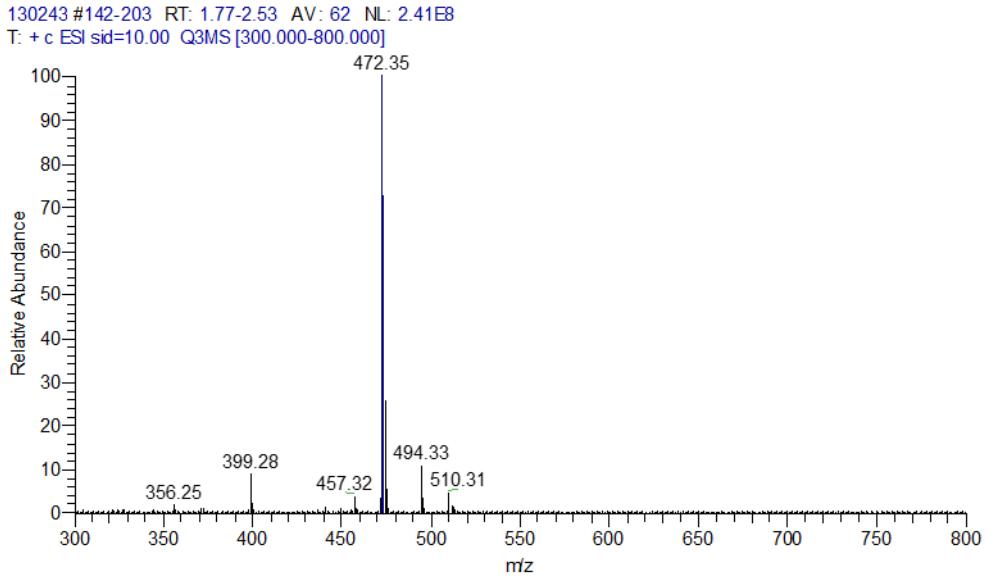

Fig. 3.27 The mass spectra of 12-(acetylthio)dodecyl 3-(3-oxyl-1,2,4,4,5-pentamethylimidazolidin-2-yl)propanoate (17).

3.4.4 Synthesis of S-10-oxo-10-(2-(1-oxyl-2,2,5,5-tetramethyl-2,5-dihydro-1H-imidazol-4-ylamino)ethylamino)decyl ethanethioate (**18**)

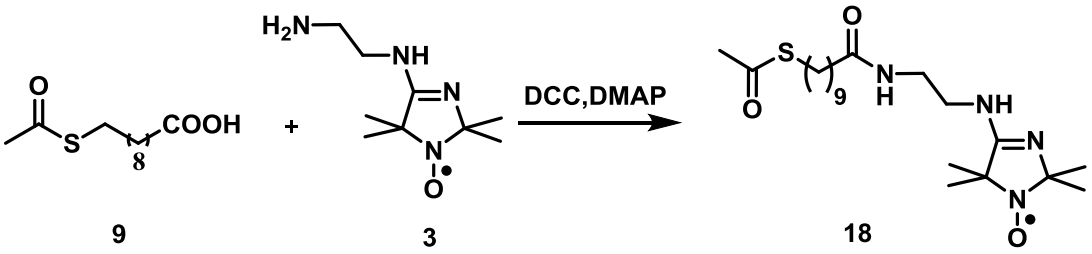

9 **3** **18**

Fig. 3.28 Scheme of the synthesis of S-10-oxo-10-(2-(1-oxyl-2,2,5,5-tetramethyl-2,5-dihydro-1H-imidazol-4-ylamino)ethylamino)decyl ethanethioate (18).

9 (100.0 mg, 4.06×10^{-4}mol), DCC (114.5 mg, 5.55×10^{-4}mol) and DMAP (1.3 mg) were dissolved in 2 mL of dry chloroform , and a solution of **3** (73.6 mg, 3.70×10^{-4}mol) in 0.5 mL of dry chloroform was added slowly to the mixture. The reaction mixture was stirred at room temperature for 24 hrs, concentrated under reduced pressure and separated by PTLC on silica gel (eluent: methanol/chloroform, 1:200).

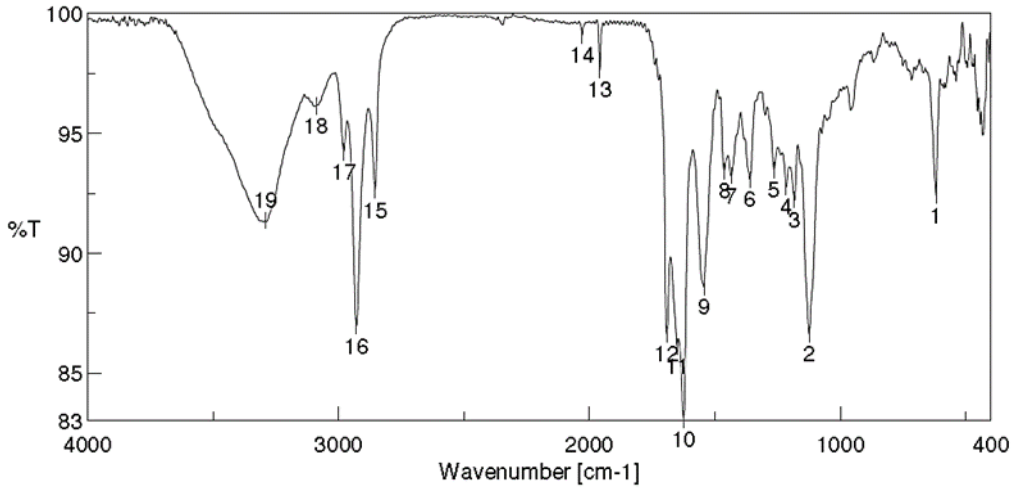

Fig. 3.29 IR spectrum of S-10-oxo-10-(2-(1-oxyl-2,2,5,5-tetramethyl-2,5-dihydro-1H-imidazol-4-ylamino)ethylamino)decyl ethanethioate (18). An absorption band at 1624 cm^{-1} (band # 10) was assigned to the stretch vibration of the conjugated C=N bond of the amidine functionality. An absorption band at 1650 cm^{-1} (band # 11) was assigned to the C=O stretch absorption of the amide group. A band # 12 at 1692 cm^{-1} was assigned to the stretch vibration of the C=O bond in the thioacetyl group.

Structure of the **18** was also verified by mass spectroscopy. Mass spectrum: calcd for $C_{21}H_{39}N_4O_3S$ 427.27 (M^+), found 428.29 $(M+H)^+$ (Fig. 3.30).

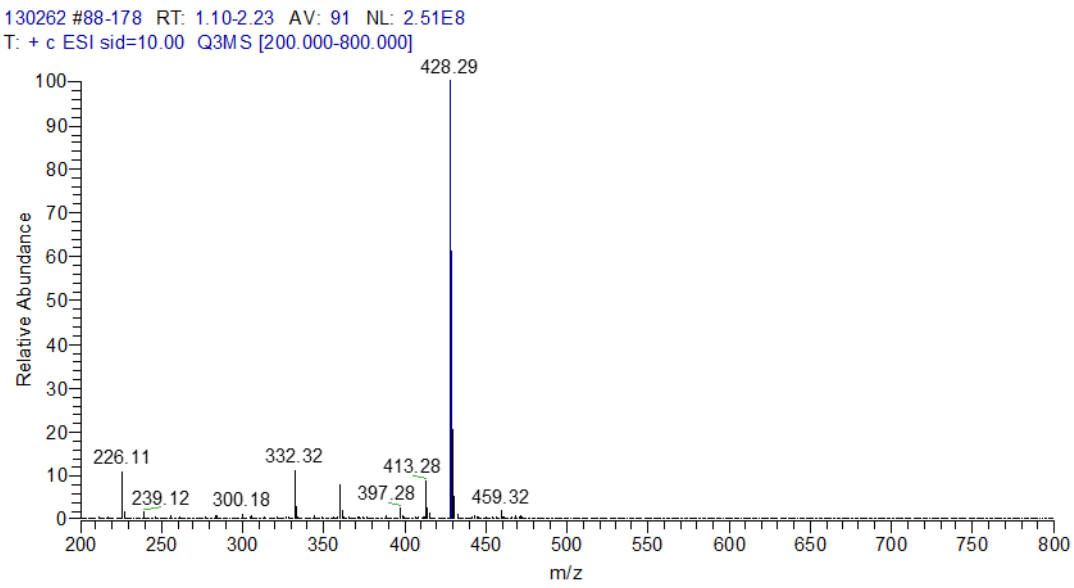

Fig. 3.30 Mass spectrum of S-10-oxo-10-(2-(1-oxyl-2,2,5,5-tetramethyl-2,5-dihydro-1H-imidazol-4-ylamino)ethylamino)decyl ethanethioate (18).

3.5 Synthesis of Functionalized Au NPs

3.5.1 Synthesis of 11-(dimethylamino)undecane-1-thiol hydrochloride-coated water soluble Au NP (**19**)

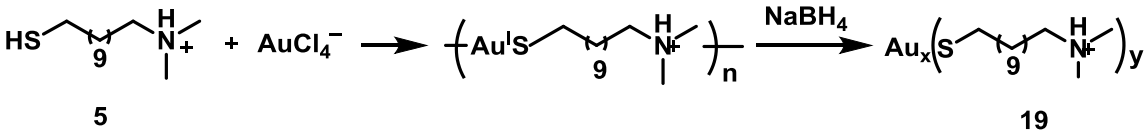

Fig. 3.31 Scheme of the synthesis of 11-(dimethylamino)undecane-1-thiol hydrochloride-coated water soluble Au NP (19).

19 was synthesized using slightly modified literature procedure. [20] Tetrachloroaurate (38.75 mg, 0.1 mmol) and **5** (80.00 mg, 0.3 mmol) were mixed in a solution of THF (5 mL) and acetic acid (0.8 mL) and stirred at room temperature overnight. Sodium

borohydride (75.00 mg, 2 mmol) was dissolved in ice-cold ultra-pure water (1.5 mL) and kept at 0 ^{o}C for 30 min and then added quickly to the ice-cold reaction mixture. The reaction mixture turned dark immediately. The reaction mixture was vigorously stirred at 0 ^{o}C for another 24 hrs. Solvents were removed under reduced pressure and the residue was re-dissolved in ultra-pure water (5 mL). A resulting solution was thoroughly filtered through the sintered glass to remove the precipitates formed, the Au NPs solution was dialyzed against ultra-pure water (4 $\times$ 1L) and lyophilized to give **19** (32.9 mg, 74.8%). Aqueous solution was freeze-dried to yield dark red powder. Coating Au NPs with **5** is verified by IR spectroscopy (Fig. 3.32).

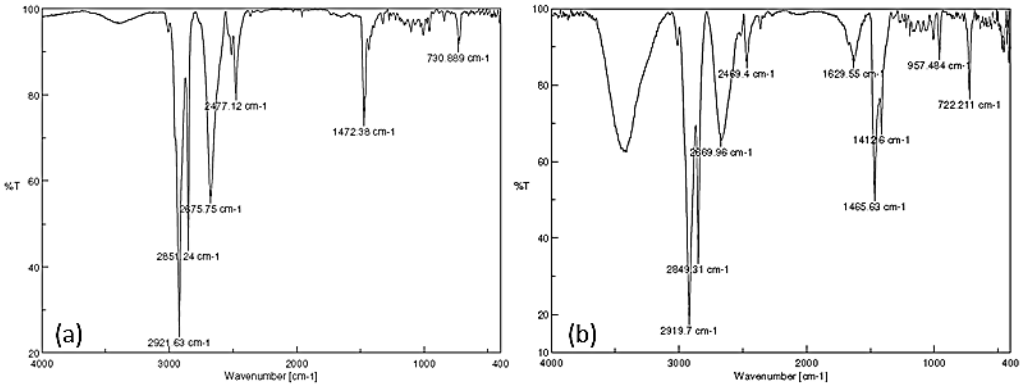

Fig. 3.32 IR spectra of (a) 5 and (b) of 11-(dimethylamino)undecane-1-thiol hydrochloride-coated water soluble Au NP (19). It can be seen that the characteristic vibration bands of 5 also present in Au NPs.

3.5.2 Synthesis of 1,2-bis(undecyl 1-oxyl-2,2,5,5-tetramethyl-2,5-dihydro-1H-pyrrole-3-carboxylate) disulfide-modified Au NPs (**20**)

Spin-labeled Au NPs were obtained through ligand exchange experiments. [20]

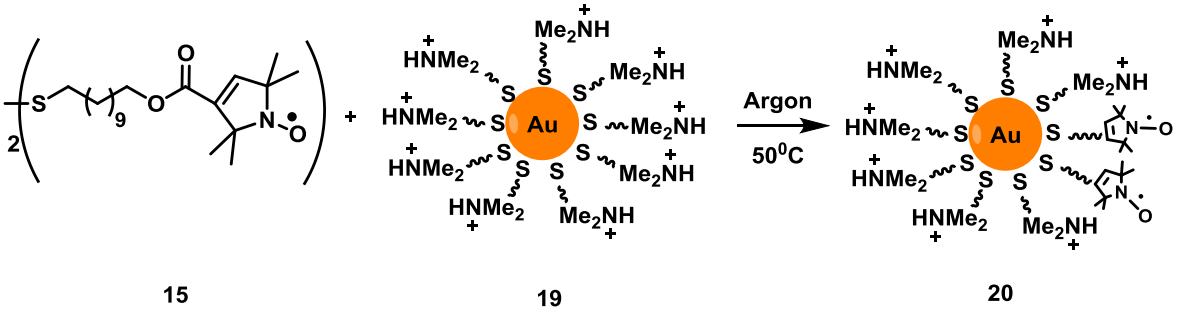

Fig. 3.33 Scheme of the synthesis of 1,2-bis(undecyl 1-oxyl-2,2,5,5-tetramethyl-2,5-dihydro-1H-pyrrole-3-carboxylate) disulfide-modified Au NPs (20).

19 (2.2 mg, 5×10^{-8} mol) were added to a solution of **15** (0.18 mg, 2.5×10^{-7} mol) in methanol (500 µL) (**15**/**19**=5:1). The mixtures were vortexed thoroughly, flushed with argon gas, and incubated under argon atmosphere at 50 ºC overnight. The solvent was evaporated under reduced pressure and the residue was re-dissolved in ultra-pure water (500 µL). Aqueous solution was extracted with dichloromethane (5×1 mL) and then dialyzed against ultra-pure water (3×500 mL) for 24 hrs to remove inorganic impurities. This ligand exchange protocol was repeated varying the molar ratio between 1**5** and **19** (e.g., 5:1, 10:1, and 20:1).

3.5.3 Synthesis of 12-(acetylthio)dodecyl 1-oxyl-2,2,5,5-tetramethyl-2,5-dihydro-1H-pyrrole-3-carboxylate-modified Au NPs (**21**).

Spin-labeled Au NPs were obtained through ligand exchange experiments. [20]

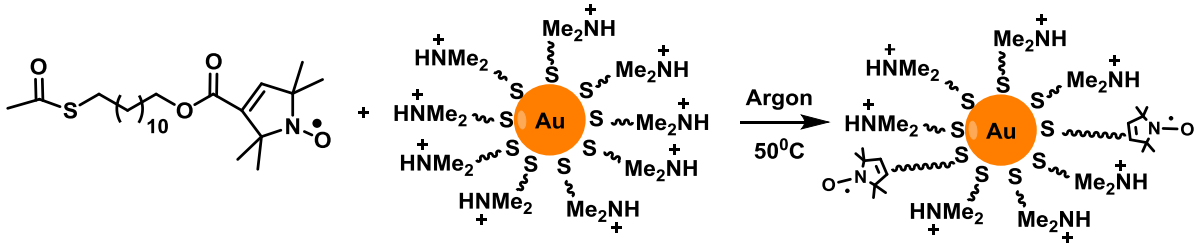

16 19 21

Fig. 3.34 Scheme of synthesis of 12-(acetylthio)dodecyl 1-oxyl-2,2,5,5-tetramethyl-2,5-dihydro-1H-pyrrole-3-carboxylate-modified Au NPs (21).

19 (2.2 mg, 5×10^{-8} mol) were added to a solution of **16** (0.855 mg, 2×10^{-6} mol) in methanol (500 µL) (**16**/**19**=20:1). The reaction mixture was vortexed thoroughly, flushed with argon gas, and incubated under argon atmosphere at 50 ^{o}C overnight. The solvent was evaporated under reduced pressure, and the residue was re-dissolved in ultra-pure water (500 µL). Aqueous solution was extracted with dichloromethane (5×1 mL) and then dialyzed against ultra-pure water (3×500 mL) for 24 hrs to remove inorganic impurities. This ligand exchange protocol was repeated varying the molar ratio between **16** and **19** (e.g., 40:1, 20:1, 10:1).

3.5.4 Synthesis of 12-(acetylthio)dodecyl 3-(3-oxyl-1,2,4,4,5-pentamethylimidazolidin-2-yl)propanoate-modified Au NPs (**22**).

Spin-labeled Au NPs were obtained through ligand exchange experiments. [20]

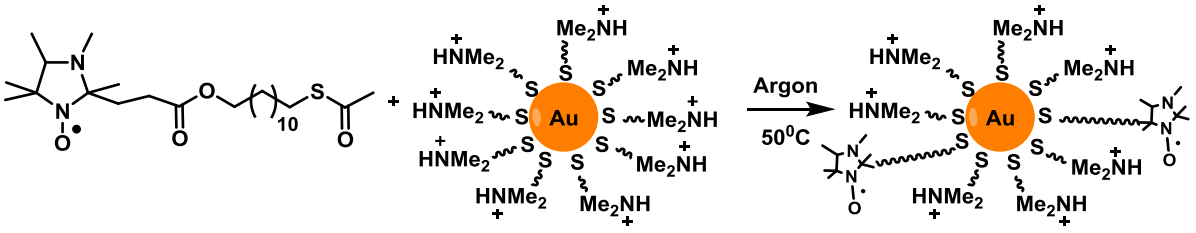

17 19 22

Fig. 3.35 Scheme of synthesis of 12-(acetylthio)dodecyl 3-(3-oxyl-1,2,4,4,5-pentamethylimidazolidin-2-yl)propanoate-modified Au NPs (22).

19 (2.2 mg, 5×10^{-8} mol) were added to a solution of **17** (0.24 mg, 5×10^{-7} mol) in methanol (500 µL) **17**/**19**=10:1). The reaction mixture was vortexed thoroughly, flushed with argon gas, and incubated under argon atmosphere at 50 °C overnight. The solvent was evaporated under reduced pressure, and the residue was re-dissolved in ultra-pure water (500 µL). Aqueous solution was extracted with dichloromethane (5×1 mL) and then dialyzed against ultra-pure water (3×500 mL) for 24 hrs to remove inorganic impurities.

3.5.5 Synthesis of S-10-oxo-10-(2-(1-oxyl-2,2,5,5-tetramethyl-2,5-dihydro-1H-imidazol-4-ylamino)ethylamino)decyl ethanethioate-modified Au NPs (**23**)

Spin-labeled Au NPs were obtained through ligand exchange experiments. [20]

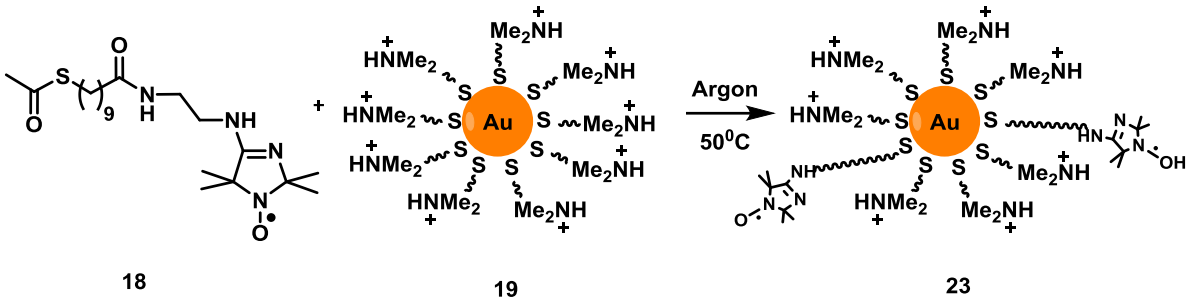

Fig. 3.36 Scheme of synthesis of S-10-oxo-10-(2-(1-oxyl-2,2,5,5-tetramethyl-2,5-dihydro-1H-imidazol-4-ylamino)ethylamino)decyl ethanethioate-modified Au NPs (23).

19 (2.2 mg, 5×10^{-8} mol) were added to a solution of **18** (0.85 mg, 2×10^{-6} mol) in methanol (50 µL) **18**/**19**=40:1). High concentrations of **19** and **18** could highly improve the ligand exchange efficiency. The reaction mixture was vortexed thoroughly, flushed with argon gas, and incubated under argon atmosphere at 50 ^{o}C overnight. The solvent was evaporated under reduced pressure, and the residue was re-dissolved in ultra-pure water (500 µL). Aqueous solution was extracted with dichloromethane (10×1 mL) and then dialyzed against ultra-pure water (3×500 mL) for 24 hrs to remove inorganic impurities.

REFERENCES

1. You, C.-C.; Chompoosor, A.; Rotello, V. M., The biomacromolecule-nanoparticle interface. *Nano Today* **2007,** *2* (3), 34-43.

2. Moyano, D. F.; Rotello, V. M., Nano meets biology: structure and function at the nanoparticle interface. *Langmuir* **2011,** *27* (17), 10376-10385.

3. McIntosh, C. M.; Esposito, E. A.; Boal, A. K.; Simard, J. M.; Martin, C. T.; Rotello, V. M., Inhibition of DNA transcription using cationic mixed monolayer protected gold clusters. *Journal of the American Chemical Society* **2001,** *123* (31), 7626-7629.

4. Atkins, P.; De Paula, J., *Atkins' physical chemistry*. Oxford University Press: 2010.

5. Brust, M.; Walker, M.; Bethell, D.; Schiffrin, D. J.; Whyman, R., Synthesis of thiol-derivatised gold nanoparticles in a two-phase liquid–liquid system. *J. Chem. Soc., Chem. Commun.* **1994,** (7), 801-802.

6. (a) Yang, H.; Kwon, Y.; Kwon, T.; Lee, H.; Kim, B. J., 'Click'Preparation of CuPt Nanorod-Anchored Graphene Oxide as a Catalyst in Water. *small* **2012,** *8* (20), 3161-3168; (b) Tien, J.; Terfort, A.; Whitesides, G. M., Microfabrication through electrostatic self-assembly. *Langmuir* **1997,** *13* (20), 5349-5355.

7. (a) Woehrle, G. H.; Warner, M. G.; Hutchison, J. E., Ligand exchange reactions yield subnanometer, thiol-stabilized gold particles with defined optical transitions. *The Journal of Physical Chemistry B* **2002,** *106* (39), 9979-9981; (b) Warner, M. G.; Reed, S. M.; Hutchison, J. E., Small, water-soluble, ligand-stabilized gold nanoparticles synthesized by interfacial ligand exchange reactions. *Chemistry of materials* **2000,** *12* (11), 3316-3320.

8. Woehrle, G. H.; Brown, L. O.; Hutchison, J. E., Thiol-functionalized, 1.5-nm gold nanoparticles through ligand exchange reactions: Scope and mechanism of ligand exchange. *Journal of the American Chemical Society* **2005,** *127* (7), 2172-2183.

9. Guo, R.; Song, Y.; Wang, G.; Murray, R. W., Does core size matter in the kinetics of ligand exchanges of monolayer-protected Au clusters? *Journal of the American Chemical Society* **2005,** *127* (8), 2752-2757.

10. Wu, Z.; Suhan, J.; Jin, R., One-pot synthesis of atomically monodisperse, thiol-functionalized Au25 nanoclusters. *Journal of Materials Chemistry* **2009,** *19* (5), 622-626.

11. (a) Dharmaratne, A. C.; Krick, T.; Dass, A., Nanocluster size evolution studied by mass spectrometry in room temperature Au25 (SR) 18 synthesis. *Journal of the American Chemical Society* **2009,** *131* (38), 13604-13605; (b) Parker, J. F.; Weaver, J. E.; McCallum, F.; Fields-Zinna, C. A.; Murray, R. W., Synthesis of Monodisperse [Oct4N+][Au25 (SR) 18−] Nanoparticles, with Some Mechanistic Observations. *Langmuir* **2010,** *26* (16), 13650-13654.

12. Chen, S.; Templeton, A. C.; Murray, R. W., Monolayer-protected cluster growth dynamics. *Langmuir* **2000,** *16* (7), 3543-3548.

13. Wallace, T. J., Reactions of thiols with sulfoxides. I. Scope of the reaction and synthetic applications. *Journal of the American Chemical Society* **1964,** *86* (10), 2018-2021.

14. Zeynizadeh, B., Oxidative coupling of thiols to disulfides with iodine in wet acetonitrile. *Journal of Chemical Research* **2002,** *2002* (11), 564-566.

15. Neises, B.; Steglich, W., Simple method for the esterification of carboxylic acids. *Angewandte Chemie International Edition in English* **1978,** *17* (7), 522-524.

16. Okabayashi, Y., Synthesis of azide- and alkyne-terminated alkane thiols and evaluation of their application in Huisgen 1,3-dipolar,cycloaddition ("click") reactions on gold surfaces. *Linköping University* **2009,** (38).

17. Khramtsov, V.; Weiner, L.; Eremenko, S.; Belchenko, O.; Schastnev, P.; Grigor'ev, I.; Reznikov, V., Proton exchange in stable nitroxyl radicals of the imidazoline and imidazolidine series. *Journal of Magnetic Resonance (1969)* **1985,** *61* (3), 397-408.

18. Reznikov, V.; Volodarskii, L., Synthesis of bifunctional derivatives of nitroxyl radicals of imidazoline. *Chemistry of Heterocyclic Compounds* **1990,** *26* (6), 643-648.

19. (a) Ionita, P.; Caragheorgheopol, A.; Gilbert, B. C.; Chechik, V., EPR study of a place-exchange reaction on Au nanoparticles: Two branches of a disulfide molecule do not adsorb adjacent to each other. *Journal of the American Chemical Society* **2002,** *124* (31), 9048-9049; (b) Chechik, V.; Wellsted, H. J.; Korte, A.; Gilbert, B. C.; Caldararu, H.; Ionita, P.; Caragheorgheopol, A., Spin-labelled Au nanoparticles. *Faraday Discussions* **2004,** *125*, 279-291.

20. Khlestkin, V. K.; Polienko, J. F.; Voinov, M. A.; Smirnov, A. I.; Chechik, V., Interfacial surface properties of thiol-protected gold nanoparticles: a molecular probe EPR approach. *Langmuir* **2008,** *24* (3), 609-612.

21. Parker, J. F.; Fields-Zinna, C. A.; Murray, R. W., The Story of a monodisperse gold nanoparticle: Au25L18. *Accounts of chemical research* **2010,** *43* (9), 1289-1296.

22. Häkkinen, H., The gold-sulfur interface at the nanoscale. *Nature Chemistry* **2012,** *4* (6), 443-455.

23. Lopez-Acevedo, O.; Akola, J.; Whetten, R. L.; Grönbeck, H.; Häkkinen, H., Structure and bonding in the ubiquitous icosahedral metallic gold cluster Au144 (SR) 60. *The Journal of Physical Chemistry C* **2009,** *113* (13), 5035-5038.

24. Huang, X.; Bronstein, L. M.; Retrum, J.; Dufort, C.; Tsvetkova, I.; Aniagyei, S.; Stein, B.; Stucky, G.; McKenna, B.; Remmes, N., Self-assembled virus-like particles with magnetic cores. *Nano letters* **2007,** *7* (8), 2407-2416.

25. Beulen, M. W.; Kastenberg, M. I.; van Veggel, F. C.; Reinhoudt, D. N., Electrochemical stability of self-assembled monolayers on gold. *Langmuir* **1998,** *14* (26), 7463-7467.

26. Sankaram, M.; Brophy, P. J.; Jordi, W.; Marsh, D., Fatty acid pH titration and the selectivity of interaction with extrinsic proteins in dimyristoylphosphatidylglycerol dispersions. Spin label ESR studies. *Biochimica et Biophysica Acta (BBA)-Biomembranes* **1990,** *1021* (1), 63-69.

27. Voinov, M. A.; Rivera-Rivera, I.; Smirnov, A. I., Surface Electrostatics of Lipid Bilayers by EPR of a pH-Sensitive Spin-Labeled Lipid. *Biophysical journal* **2013,** *104* (1), 106-116.

28. Pillai, P. P.; Huda, S.; Kowalczyk, B.; Grzybowski, B. A., Controlled pH Stability and Adjustable Cellular Uptake of Mixed-Charge Nanoparticles. *Journal of the American Chemical Society* **2013,** *135* (17), 6392-6395.

29. Smirnov, A. I.; Belford, R. L., Rapid quantitation from inhomogeneously broadened EPR spectra by a fast convolution algorithm. *Journal of Magnetic Resonance, Series A* **1995,** *113* (1), 65-73.